Clinically relevant concurrent BRAF and MEK inhibition alters differentiation states and sensitizes BRAF V600E-mutated high-grade gliomas to immune checkpoint blockade

Authors: Jong-Whi Park[1,2,†], Stefan Grossauer[3,4†], Wei Wang[2,5], Yao Lulu Xing[1], Katharina Koeck[4], Cesar A. Garcia[1], Emon Nasajpour[1], Christy Wilson[1], Hope Lancero[1], Patrick N. Harter[6], Katharina Filipski[7], Mathieu Daynac[2,8], Lasse Meyer[1,9, 10], Maria Isabel Barros Guinle[1], Michelle Monje[10], Hannes Vogel[11], Michael Lim[1], Laura M. Prolo[1], Gerald A. Grant[1,12], and Claudia K. Petritsch[1,*]

Affiliations:

[1]Department of Neurosurgery, Stanford University School of Medicine, Palo Alto, CA94305, USA.

[2]Present address: Department of Life Sciences, Gachon University, Incheon 21999, South Korea

[3]Department of Neurosurgery, University of California San Francisco, San Francisco, CA94143, USA

[4]Present address: Medical University of Vienna, Department of Neurosurgery, A-1090 Vienna, Austria.

[5]Department of Neurosurgery, The First Affiliated Hospital of Xi'an Jiaotong University; Xi'an, China.

[6]Center for Neuropathology and Prion Research, University Hospital of Munich, LMU Munich, Munich Germany

[7]Neurological Institute (Edinger Institute), University Hospital, Frankfurt, Frankfurt am Main, Germany

[8]Present address: Department of Bioengineering and Therapeutic Science, University of California San Francisco, San Francisco, CA94143, USA

[9]German Cancer Research Center, DKFZ, Heidelberg, Germany

[10]Present address: Department of Quantitative Biomedicine, University of Zurich, Zurich, CH-8093, Switzerland

[11]Departments of Neurology and Neurological Sciences, Stanford University School of Medicine, Palo Alto, CA94305, USA.

[12]Department of Pathology, Stanford University School of Medicine, Palo Alto, CA94305,

[13]Present address: Department of Neurosurgery, Duke University School of Medicine, Durham, NC 27710, North Carolina

[†]These authors contributed equally.

*** Corresponding Author:** Claudia K. Petritsch; Lorry I. Lokey Stem Cell Research Building, Stanford University School of Medicine, 265 Campus Drive, Room G1169, Palo Alto, CA94305; Email: cpetri@stanford.edu (C.K.P.)

Running title: BRAF V600E-mutated glioma treatment with clinically relevant dual MAPK pathway inhibitors alters tumor cell differentiation and immune infiltrate and sensitizes to dual immune checkpoint blockade in a T cell-dependent manner.

Keywords: BRAF-mutated glioma, MAPK pathway inhibitors, immune checkpoint blockade

Additional Information

Manuscript total word count:

Total number of figures: 7 in main manuscript plus 7 supplemental

Total number of tables: 2 in main manuscript plus 3 in supplemental

ABSTRACT

BRAF V600E-mutated glioma patients are in urgent need of new treatments, since standard chemoradiotherapy and surgery achieves tumor control in less than 30% of patients. BRAF and MEK inhibitor combinations have shown promising results against several types of BRAF V600E mutated cancers. Patients with high-grade BRAF V600E mutated gliomas frequently experience therapy failure with concurrent BRAF V600E and MEK inhibition (BRAFi+MEKi). Overcoming therapy resistance begins with understanding how these inhibitors affect tumor cells and the immune microenvironment. In novel syngeneic murine models and patient-derived cell lines of BRAF V600E-mutated high-grade astrocytomas, we analyzed effects of BRAF V600E expression and BRAF V600E inhibitor Dabrafenib and MEK inhibitor Trametinib (BRAFi+MEKi). BRAF V600E expression disrupted asymmetric cell division and glial differentiation, and BRAFi+MEKi restored these defects, and enriched for potentially therapy resistant CD133+ tumor cells. Increased interferon alpha and gamma signatures and pro-inflammatory cytokines were detected. Programmed death (PD-1) receptor ligand was found to be expressed in murine and human BRAF V600E mutated high-grade gliomas, and BRAFi+MEKi upregulated the frequency of tumor-infiltrating T cells expressing inhibitory immune checkpoints, suggestive of T cell exhaustion. Combining dual MAPK pathway with immune checkpoint inhibition by anti-PD-L1 and anti-CTLA-4 treatment decreased T cell deactivation and resulted in a T cell-dependent survival benefit of mice with orthotopic BRAF V600E-mutated high-grade gliomas. These data showed that clinically relevant dual MAPK pathway inhibition sensitized high-grade gliomas to the anti-tumor activity of concurrent dual immune checkpoint blockades. Therefore, we propose that in patients with BRAF V600E high-grade gliomas, improved therapeutic benefits could be derived from combining BRAFi+MEKi with immune checkpoint inhibitors.

INTRODUCTION

Cancers of the central nervous system (CNS) are the leading cause of death by disease in children aged 0-14 years in the United States [1, 2]. Large-scale genomic analyses identified key differences in pediatric and adult tumors [3-6], with pediatric gliomas predominantly harboring genetic alterations that converge on growth factor activated RAS/RAF/mitogen-activated protein kinase (MAPK) pathway [6-9]. The V-Raf murine viral oncogene homolog B1 (BRAF) is a proto-oncogene. BRAF V600E is the most frequent mutation in BRAF; it is generated by a substitution of valine to glutamate at position 600 resulting from a point mutation within exon 15 of the BRAF kinase gene (c.1799T>A). This mutation switches BRAF kinase monomers to an active configuration and thereby pathologically activates kinase activity 500-fold and decouples it from upstream growth factor and RAS activity [10, 11]. BRAF V600E constitutively activates the MAPK signaling pathway, which is mainly known for promoting cell growth and proliferation of cancer cells but has also been associated with senescence, cell fate changes, and differentiation [12, 13].

The BRAF V600E mutation occurs in 6.5% of all patients with glioma, a CNS cancer. It is enriched in the epithelioid GBM subtype (69%) [14] and in pediatric gliomas across several histologic subtypes. Incidences range from high occurrences in low-grade gliomas to low occurrences in high-grade gliomas (<5%). BRAF V600E is particularly common in pleomorphic xanthoastrocytoma (PXA, 56%), and ganglioglioma (GG, up to 60%). The majority of pediatric CNS tumors are low-grade gliomas [15, 16] with overall similar favorable outcomes [17]. BRAF V600E expression however correlates with poor survival amongst these tumors (20-year progression-free survival (PFS) <30%) compared with BRAF V600E wildtype at 58%)[6, 18].

Concomitant alterations in BRAF V600E and CDKN2A loss are associated with a higher risk of progression, malignant transformation, and overall poorer outcomes [6, 19-21]. When progressed to a high grade, gliomas uniformly exhibit resistance to standard chemoradiation therapy [22]. Overall, tumor grade is a strong predictor of poor outcome in pediatric patients with BRAF V600E-mutated glioma with a progression-free survival at one year at 27% for high-grade gliomas versus 86.4% for low-grade gliomas [9]. Although BRAF V600E high-grade gliomas have better clinical outcomes compared with high-grade gliomas marked by mutations in receptor tyrosine kinases (RTKs) and Histone 3 (H3) [23], they are unrelenting tumors. Therefore, BRAF V600E-mutated glioma patients are in urgent need of new treatment, since standard chemoradiotherapy and surgery achieves tumor control in less than 30% of patients despite multiple rounds of treatment [24, 25].

Identification of the actionable BRAF V600E mutation in a variety of cancers (most prominently metastatic melanoma, hairy cell leukemia, serous borderline ovarian cancer, and thyroid carcinoma [11, 26]), led to FDA development and approval of BRAF inhibitors [27-30], and later the combination of BRAF and MEK inhibitors, including Dabrafenib plus Trametinib [31], for the treatment of BRAF-mutant non-CNS cancers. These orally bioavailable small molecule inhibitors of BRAF have shown high response rates in BRAF V600E solid cancer and are FDA-approved for targeting the mutant kinase in melanoma, papillary thyroid cancer, and non-small cell lung cancer and hairy cell leukemia. BRAF inhibition improves survival in melanoma [28] and has broad clinical activity in non-melanoma cancer, with clear tumor type-dependent differences in efficacy [32-39]. Driven by strong preclinical data in gliomas, including from our laboratory [40-42], patients with BRAF V600E-mutated gliomas are good candidates for treatment with pharmacologic BRAF V600E inhibitors (BRAFi). Continuous suppression of MAPK pathway correlates with clinical efficacy [27], but the therapeutic effects of BRAF inhibitors are however

mostly transient, which is why they are frequently combined with small molecule inhibitors of downstream kinase MEK [9, 36, 37, 39, 43, 44]. Multiple studies indeed suggested that the combination of pharmacologic BRAF V600E and MEK inhibition (BRAFi+MEKi) is superior to BRAF inhibitor monotherapy in melanoma, and non-melanoma cancers [42-51]. The combination of BRAFi+MEKi (e.g., Dabrafenib plus Trametinib) demonstrated promising efficacy when compared with BRAFi monotherapy in gliomas [43, 52, 53]. Several ongoing clinical trials report a much higher objective response rate in low-grade (80%) versus high-grade gliomas (25%-36%) [9, 38, 50, 54], suggesting a significant improvement with BRAFi+MEKi over standard therapy, especially for low-grade tumors.

Tumor rebound after treatment discontinuation, and drug resistance, are two concerning complications of BRAFi+MEKi in glioma and complete responses in BRAF V600E-mutated gliomas are rare, especially in high-grade tumors [9, 23, 35, 38, 42-45, 48, 55-57]. Therefore, additional therapies that increase anti-tumor efficacy and overcome resistance are urgently needed. In melanoma, BRAF V600E expression and BRAF and MEK inhibition reportedly abrogates an immunosuppressive tumor microenvironment by multiple mechanisms; these include upregulation of melanoma differentiation antigen expression and decrease in expression of immunosuppressive factors. BRAFi+MEKi suppresses myeloid-derived suppressor cells, regulatory T cells, and increases macrophages, and augments a T cell infiltrate and function in melanoma mouse models and patient [58-66]. In addition to molecular-targeted therapies, therapeutic antibodies designed to block inhibitory immune checkpoints are highly successful in BRAF V600E mutant melanoma; in particular, the targeting of programmed cell death (PD)-1, a receptor that maintains peripheral immune tolerance by fine tuning T-cell responses [67]. These two therapeutic modalities are

therefore tested in combination in the clinical setting. The potential effects of BRAFi+MEKi, including potential changes in the immune infiltrate of pediatric BRAF V600E mutant gliomas, remain to be assessed. The scarcity of patient-derived cell lines for BRAF V600E mutated high-grade gliomas combined with the histopathologic and genetic diversity of BRAF V600E mutated gliomas creates a challenge for experimental therapeutics of this disease. Thus, developing and refining preclinical mouse models for BRAF V600E mutated tumors is critical. BRAF V600E expression in mouse brain cells induces formation of high-grade gliomas but only when combined with additional oncogenic alterations, such as activated Akt, loss of tumor suppressors Tp53, or loss of tumor suppressor locus Ink4a/Arf, the mouse homolog of the *CDKN2A* locus [41, 68].

We investigated the effects of BRAFi+MEKi by Dabrafenib and Trametinib in a new syngeneic mouse model and patient-derived cell lines representing BRAF V600E-mutated high-grade gliomas. To faithfully recapitulate the genetic alterations found in human tumors we induced expression of BRaf V600E and concomitant deletion of Ink4a/Arf, the murine CDKN2A locus in mice. When targeted to hemispheric regions where human tumors are commonly located these alterations consistently led to tumor formation, recapitulating the neuroanatomical preference of BRAF V600E-mutated CDKN2A-deleted human gliomas. Up-regulation of a CD133+ cell population and *CD133* mRNA expression, after BRAFi+MEKi treatment were observed in the murine glioma and patient-derived cell lines; this is indicative of this population's involvement in therapy escape. In murine and human tumor cells, BRAFi+MEKi reverted asymmetric cell division and differentiation defects induced by BRAF V600E expression. RNA expression profiling and validation by quantitative rtPCR revealed increased interferon alpha and gamma signatures and pro-inflammatory cytokines in response to BRAFi+MEKi and up-expression of

immune checkpoint and negative T cell regulator program-death receptor (PD-1) signaling. Cytometry analyses showed heightened frequency of PD-1-positive tumor-infiltrating T cells after prolonged (14 days) BRAFi+MEKi treatment. Concurrent immune checkpoint inhibition with anti-PD-L1 and anti-CTLA-4 antibodies combined with BRAF plus MEK inhibitors increased survival of murine glioma-bearing mice in a T-cell-dependent manner. In summary, our studies have improved our understanding of BRAF V600E-mutated CDKN2A-deleted glioma development and treatment; we believe they warrant further translational studies that focus on testing immune checkpoint blockades as a novel therapeutic approach for this tumor entity.

RESULTS

A novel mouse model recapitulates neuroanatomic location and intra-tumoral cellular heterogeneity of BRAF V600E-mutated CDKN2A-deleted gliomas

BRAF V600E frequently co-occurs with additional genetic alterations in glioma, most commonly deletion of CDKN2A, which is found in 9.6% of BRAF V600E mutated low-grade [6] and 57-58% of BRAF V600E mutated high-grade gliomas [6, 20, 21, 41, 55, 56]. BRAF V600E cases occur most frequently in the cerebral hemispheres and at lower frequencies in the midline [41, 42, 68-70]. To recapitulate the genetic and neuroanatomical preferences of these tumors, we first tested if expression of BRAF V600E and deletion of CDKN2A in hemispheric areas gives rise to high-grade gliomas in mice. We generated compound transgenic mice carrying a cre-activated knock-in allele (BRaf CA) [71], the knock-out allele for the murine Cdkn2a homologous locus Ink4a/Arf (Ink4a/Arf flox/flox) **(Figs. S1A and B),** and for selected experiments the Rosa26-LacZ reporter strain [72]. Compound transgenic mice were injected with adenovirus encoding Cre recombinase (Ad::Cre) into the inner cortical layers V-VI (CX I) adjacent to the white matter area of the corpus

callosum (CC) and the outer cortical layers I-IV (CX II) to activate BRaf V600E expression and Cdkn2a deletion **(Figs. 1A and S1C)**.

Ad::Cre injection into BRaf CA Ink4a/Arf flox/flox mice shortened survival of all animal subjects, when compared with BRaf CA/WT Ink4a/Arf wildtype (WT) mice and Ad-GFP injected mice as controls (**Fig. 1A**) [41]. Successful injection and cre-mediated recombination in target areas was confirmed using the beta-galactosidase (beta-gal) reporter assays **(Figs. 1B and S1D)**. Immunohistopathologic analyses by hematoxylin and eosin (HE) staining of mouse brains detected diffuse tumors in hemispheric, cortical regions adjacent from the injection sites. We noted that tumors infiltrated the cortex but rarely crossed the white matter area of the corpus callosum upon cortical injection. Non-specific spindle cell proliferation and necrosis were consistent with high-grade astrocytomas (**Figs. 1B and S1D**).

To further characterize tumor cells, we performed immunostaining for neural stem and progenitor and glial cell markers and beta-galactosidase as a marker for tumor cells [40]. Astrocyte marker glial fibrillary acidic protein (GFAP) expression was detected that was consistent with astrocytoma histology. In addition, GFAP-positive cells lacking beta-gal expression were also detected in the periphery, consistent with reactive astrocytes **(Fig. 1C**). Tumor cells are highly positive for oligodendrocyte and pan-glioma marker Olig2 [73], and to a lesser extent express neuronal progenitor marker Nestin **(Fig. 1D)** and OPC marker NG2 **(Fig. 1E)**. Tumor areas were also positive for phospho-ERK, indicative of constitutive MAPK pathway activity in response to BRAF V600E expression **(Fig. 1E)**. Lastly, cell dissociates from endogenous BRaf V600E-mutated Cdkn2A-deleted tumors were modified *in vitro* with lentivirus-luciferase-GFP and injected intracranially, which led to formation of high-grade gliomas. Orthotopic tumor cells invaded white matter areas, as demonstrated by intermixing of GFP-positive tumor cells with NG2-positive GFP-

negative resident OPCs **(Fig. 1F)**. Like endogenous tumors, orthotopic tumors expressed GFAP and Olig2 **(Figs. S1E and S1F)**. In addition, we detected tumor cells positive for CD133/Prom1, a marker for cancer stem cells and newly formed oligodendrocytes [74]. The percentage of CD133/Prom1-positive cells amongst Ki67-positive cells was significantly lower than that of Olig2-positive cells (%Ki67/Olig2+= 64.4%; %; vs. %Ki67/CD133+ = 19.4%; $p<0.0001$), indicative that the CD133/Prom1 cells have a lower proliferation rate than the bulk of tumor cells **(Fig. 1G-I).** These data revealed intra-tumoral heterogeneity consistent with our earlier study which indicated that human BRAF V600E-mutated CDKNA-deleted high-grade gliomas consist of several phenotypically distinct subpopulations [40]. Collectively, these data showed that BRaf V600E expression and CDKN2A deletion in young adult mice generated infiltrative high-grade astrocytoma in cortical and white matter areas, reminiscent of human high-grade tumors carrying these genetic alterations. (**Fig. 1G and H**).

Oncogenic MAPK pathway activation elicited diverse cellular responses partially reversible by BRAF and MEK inhibitors.

BRAF V600E expression in human neural stem cells induces transformation and then senescence and increases glial progenitor cell frequency and seizures in embryonic brains [12, 75]. The effect of BRAF V600E on CDKN2A-deleted postnatal neural stem cells has not been assessed. We investigated the effects of BRaf V600E expression by inducing its expression in CDKN2A-deleted cells (denoted Ink -/-) in murine neurospheres derived from the subventricular zone of young adult brains. We quantified the changes in percentages of progenitor and glial cells in response to BRAF V600E expression first by flow cytometry. The percentage of NG2+ cells in neurospheres was higher than that of CD133/Prom1+ and was significantly elevated by BRaf V600E expression in

Ink -/- neurospheres. The percentage of CD133+ cells was similar in BRaf V600E Ink -/- and BRaf WT Ink-/- neurosphere cultures and was overall significantly lower than that of NG2+ cells in BRaf V600E Ink -/- neurospheres **(Fig. 2A)**. These data are consistent with the low frequency of CD133+ cells we previously observed in established human BRAF V600E-mutated cancer cell lines [54]. BRaf V600E increased the frequency of cells immunoreactive for the intermediate filament protein Nestin, that is normally expressed in neural progenitor cells and reactive astrocytes, and the glycolipid A2B5, that is normally expressed on multipotent oligodendrocyte progenitor cells and tumor initiating as well as glioma cells **(Fig. 2B and 2C)** [76]. The increase in OPC-like cells was confirmed by immunocytochemistry on dissociated cell neurospheres, which revealed a higher percentage of NG2+ and Olig2+ cells **(Figs. 2D, 2E, S2A, S2C and S2D)**; this is concurrent with a lower percentage of differentiated oligodendrocytes, identified by myelin basic protein (MBP) expression and astrocytes, identified by glial fibrillary acidic protein (GFAP) expression **(Figs. 2D, 2E, S2A and S2B)**, and nuclear Olig2+ in BRaf V600E Ink -/- vs. BRaf WT Ink -/- cells **(Fig. S2C and S2D)** [77]. Interestingly, five-day treatment with pharmacologic BRAF V600E inhibitor PLX4720 and MEK inhibitor PD90859 decreased the percentage of nuclear Olig2+ cells **(Figs. S2C and S2D)**, concurrent with a significant higher percentage of GFAP+ astrocytes in BRAF inhibitor (BRAFi) treated neurospheres (**Fig. S2E**). These data indicated that BRAF inhibitors not only block proliferation and increases apoptosis of glioma cells, as previously reported [42], but also restore differentiation towards astrocytes and oligodendrocyte lineage cells that has been disrupted by BRAF V600E expression.

Next, we tested whether clinically relevant BRAF and MEK inhibitor combinations Dabrafenib plus Trametinib affect differentiation states of glioma cells. Murine BRaf V600E Ink -/- glioma-derived cells incubated with BRAFi + MEKi Dabrafenib plus Trametinib (D+T) exhibited a

differentiated branch morphology in the absence of growth factors (**Figs. 2F and 2H**). Quantifications revealed an increase in GFAP+ cells, consistent with an increase in astrocyte differentiation and differentiated morphology**,** whereas OPC-like cell morphology was altered despite no significant changes were observed in cell percentage and mean signal intensity of OPC marker NG2 **(Figs. 2G and 2I, S2F)**. To investigate potential treatment-induced changes to cell fate and differentiation states more broadly, we treated mice bearing intracranial BRaf V600E Ink -/- murine gliomas with BRAFi + MEKi (Dabrafenib plus Trametinib) for three consecutive days and enriched for glial progenitor and tumor cell marker A2B5-positive (CD133–A2B5+) cells by magnetic-activated cell sorting (**Fig. S2G**). A2B5 mRNA and protein expression are known to be enriched in BRAF-altered gliomas [78], which we confirmed by immunostaining for our BRAF V600E-mutated murine glioma cells (**Figs. 2B and 2C**). We performed bulk RNA sequencing on *ex vivo* cells from vehicle-treated and BRAFi+MEKi-treated samples. We found that in response to drug treatment transcripts for progenitor markers negatively associated with differentiation including the *cspg4* gene which encodes NG2 and *nestin* are downregulated while genes positively associated with oligodendrocyte (*cnp, cldn11, mbp*) and astrocyte (*aldoc, gfap*) differentiation are upregulated **(Fig. 2J)**.

Collectively, BRAF V600E expression increased the percentage of glial and neuronal progenitor cells and blocked glial differentiation while clinically relevant pharmacologic inhibitors of BRAF V600E and MEK reversed these cellular phenotypes and promoted glial differentiation.

Concurrent BRAFi and MEKi treatment restored oncogene-induced defects in asymmetric cell division and increased frequency of CD133+ cells lacking Nestin

We previously showed that glioma precursor cells have aberrant cell differentiation and exhibit higher rates of symmetric divisions at the expense of asymmetric cell divisions (ACD), suggesting that ACD defects are the underlying cause for oncogene-induced differentiation defects [79]. In addition, BRAFi-resistant CD133+ BRAF V600E mutated human high-grade glioma cells undergo ACD [40]. Therefore, we looked next whether BRAF V600E expression affects ACD, and whether CD133/Prom1+ is expressed in these tumors. Immunocytochemistry combined with pair assays detected asymmetrically dividing CD133/Prom1+ cells alongside NG2+ cells in murine Ink4a/Arf-deleted (Ink -/-) cells **(Figs. 3A and 3C)**. Expression of BRaf V600E reduced ACD rates and concurrently increased symmetric divisions in NG2+ cells, consistent with an increased frequency of NG2+ cells upon BRaf V600E expression **(Fig. 2A and 2E)**. In contrast, CD133/Prom1+ cells ACD rates and frequency was unaffected by BRaf V600E expression **(Figs. 3A and 3B)**. BRAFi treatment increased rates of ACD of NG2+ cells, restoring them to levels detected in BRaf WT Ink4a/Arf -/- cells **(Figs. 3C and 3D)**, consistent with a differentiated morphology **(Fig. 2F and 2G)**.

CD133 expression in high-grade astrocytoma cells has been associated with CSC features such as elevated malignant potential and therapy resistance [40, 80-82] but CD133/Prom1+ cells from BRAF V600E-mutated tumors have not yet been characterized. We used flow cytometric sorting to enrich for CD133/Prom1+ cells from resected orthotopic murine BRaf V600E Ink -/- gliomas and separated them from NG2+ cells representative of OPC-like tumor cells. Both populations were injected intracranially at 1000 cells/mouse and survival analyses of injected mice showed that CD133/Prom1+ cells have heightened malignancy compared with NG2+ glioma cells upon intracranial injection (**Figs. S3A and S3B**) (CD133+ = 60 days median survival post-injection; NG2+ = 92 days median survival post-injection; p=0.025). Despite their higher frequency, NG2+

cells isolated from murine BRaf V600E Ink -/- gliomas induced orthotopic gliomas with longer latency than CD133+ cells **(Figs. S3A and S3B)**. We also confirmed that CD133+/Prom1+ cells exhibited reduced sensitivity to the anti-proliferative effects of BRAF inhibitor consistent with their human counterparts and indicative of their role in therapy resistance (**Figs. S3C – S3E**).

In human glioblastoma cell lines, we have previously detected CD133+ BRAF V600E mutated human high-grade glioma cells that exhibit BRAFi-resistance [40]. To assess how concurrent pharmacologic inhibition of BRAF V600E and MEK (BRAFi+MEKi) affected these cells, we treated mice bearing orthotopic BRaf V600E Ink -/- gliomas for a short period (five consecutive days) with dabrafenib (BRAFi) plus MEK inhibitor trametinib (MEKi) (**Figs. 3E**). First, we determined the CD133+ cell frequency in tumors by flow cytometry and quantified overlapping expression with Nestin, a marker frequently co-expressed in CD133+ CSCs [83]. Interestingly, there was increased frequency of CD133+ cells negative for Nestin expression after BRAFi+ MEKi treatment, despite a non-significant trend for increased total CD133+ cells. Given the majority of Nestin+ cells co-expressed CD133, the frequency of Nestin+ cells were therefore significantly decreased (**Figs. 3F and 3G**).

Co-immunofluorescence for neural stem and progenitor cell markers Nestin and CD133/Prom1 in our syngeneic orthotopic murine BRaf VE Ink-/- gliomas after 14 days of consecutive treatment with Dabrafenib plus Trametinib corroborated the presence of single and double-positive cells. Nestin-positive and double-positive cells within the tumor mass were visibly reduced with treatment **(Fig. 3H).**

Overall, our findings revealed an oncogene-induced loss of ACD. Pharmacological dual inhibition of MAPK pathway signaling restored ACD defects and enriched for a distinct CD133+ cell population that is potentially implicated in BRAFi+MEKi therapy resistance .

Concurrent BRAFi and MEKi treatment increased *de novo* CD133+ expression and frequency of CD133+ cells in human BRAF V600E-mutant gliomas

Next, we tested whether clinically relevant BRAFi+MEKi treatment enriches for CD133+ cells in human BRAF V600E-mutated gliomas. A patient with a BRAF V600E-mutated high-grade glioma underwent tumor surgery, chemoradiation, and concurrent BRAFi+MEKi with Dabrafenib and Trametinib. Despite extensive treatment, the tumor recurred within two months predominantly presenting as leptomeningeal disease (**Figs. 4A, 4B, S4A and S4B; data not shown**). We first examined whether clinical BRAFi+MEKi alters CD133+ cell expression. Treatment-naïve patient-derived tumor tissue and tumor tissues collected at autopsy from the same patient (after treatment) were assessed by histopathology. A significant increase in CD133 expression was microscopically visible and confirmed by cell quantifications **(Figs. 4C and 4D).** Next, we assessed the effects treatment *CD133* mRNA expression levels in treatment-naïve cells and cells after treatment from fresh surgical tissue dissociate. We performed quantitative real-time (qRT-) PCR and found a significant increase in *CD133* mRNA levels in cells from tissue obtained from surgical material after the patient had received several rounds of treatment, when compared with that from patient-matched treatment-naïve tumor cells (**Fig. 4E**). These data suggest that heightened levels of CD133 mRNA are a direct consequence of BRAF and MEK inhibitor treatment. To investigate this hypothesis directly, we treated cells *in vitro* with BRAFi+MEKi (Dabrafenib plus Trametinib) and assessed *CD133* mRNA levels using quantitative rt-PCR **(Fig 4E)**. We indeed detected an increase in expression levels of *CD133* mRNA in the samples after treatment. We corroborated the increase in expression levels of *CD133* mRNA in two BRAF V600E-mutated adult glioblastoma cell lines (DBTRG and AM38), and an additional patient-derived pediatric

glioblastoma cell line (aGBM5). *CD133* mRNA levels did not increase in the sample from after treatment and in BRAFi-resistant cell lines (data not shown), or BRAF wildtype glioma cells (U87MG, SF188) (**Figs. 4E and 4F**, **S4C and S4D**). BRAFi+MEKi treatment did not consistently increase expression of other stemness markers such as Sox2 or Nestin (data not shown).

We next assessed the sensitivity to the anti-proliferative effects of BRAFi+MEKi using viability assays. We determined the half maximal inhibitory concentration (IC50) for the aGBM5 cell line for Dabrafenib plus Trametinib (**Fig. S4E**) and showed that cells post-treatment exhibited no sensitivity to treatment **(Fig. 4G)**.

Taken together, we found elevated *CD133* mRNA expression and a concomitant increase of CD133+ cell numbers in response to BRAFi+MEKi treatment, indicating a positive correlation between peak levels of CD133 and resistance to BRAFi+MEKi.

MAPK pathway inhibitors upregulated interferon response and MHC expression in human and mouse BRAF V600E-mutated glioma cells

Drug treatments such as BRAFi+MEKi alter the tumor immune infiltrate [61, 62, 84-86] but their effects on gliomas - known for lack of an active anti-tumor immune response and immunosuppression [87] - have yet to be investigated. To better understand the impact of BRAFi+MEKi on the tumor, we performed gene set enrichment analysis (GSEA) of RNA expression profiles of A2B5+ cells isolated from BRaf V600E Ink -/- murine glioma-bearing mice treated for five consecutive days with Dabrafenib and Trametinib, as described in **Fig. 3E**. When comparing control-treated with inhibitor-treated conditions, we found that genes upregulated by treatment were enriched in interferon alpha (IFNα) and gamma (IFNγ) response signatures (**Figs.**

5A and 5B). Although IFN-γ responses are studied in the context of tumor cell apoptosis, these interferon signal transduction pathways positively regulate major histocompatibility complex (MHC) molecule expression [88]. From Reactome pathway GSEA analysis, inhibitor treatment significantly upregulates genes involved in the MHC class I antigen presentation pathway in addition to programmed death receptor (PD-1) signaling (**Fig. 5C**). We then performed pathway visualization and identified the fold changes in genes associated with PD-1 signaling, whereby the T-cell surface glycoprotein CD3 zeta chain *Cd247*, programmed cell death protein 1 (*Pdcd1*), cluster of differentiation 4 (*Cd4*), cluster of differentiation 3 epsilon (*Cd3e*), and histocompatibility 2, class II antigen E beta 2 (*H2-Eb2*) were following treatment the significantly altered transcripts within the PD-1 signaling cascade **(Fig. 5D**). Treatment-induced upregulation of selected MHC class I and class II genes was validated by qRT-PCR in mouse BRaf V600E-mutated glioma cells *in vitro* (H2-Aa: synonym -HLA IA-alpha, and H2-Ab1: synonym-HLA IA-beta) (**Fig. 5E**). We corroborated out findings in a BRAF V600E-mutated CDKN2A-deleted patient-derived glioblastoma cell line SU-aGBM5 (**Figs. S5A and S5B**). A 67 overlapping upregulated gene signature associated with treatment-induced IFN-γ response was identified in both human and mouse BRAF V600E-mutated CDKN2A-deleted glioma lines (**Fig. S5C**). Specifically, we observed upregulated gene expression in one out of three major types of human MHC class I transmembrane proteins, HLA-B, as well as the HLA class II histocompatibility antigen DR alpha chain (HLA-DRA). In human samples, we observed upregulation of the class II transactivator (CIITA) which activates MHC class II gene expression and is a known downstream target of IFNγ **(Fig. S5D-F).** Upregulation of HLA-B, HLA-DRA, CIITA, and a second MHC class I transmembrane protein HLA-A was corroborated in a second BRAF V600E mutated high-grade glioma patient-derived cell line by qRT-PCR **(Fig. S5F**).

Therefore, we found that BRAFi+MEKi treatment elicited gene expression changes consistent with promoting CD4+CD8+ T cell response, enhanced tumor antigenicity and dampening of T cell activity by the PD-1 immune checkpoint.

BRAF V600E-mutated high-grade gliomas harbor tumor-infiltrating lymphocytes and express inhibitory immune checkpoint molecules

Earlier studies have identified higher frequency of CD3+CD8+ T cells and a lower frequency of CD3+ FOXP3+ inhibitory, regulatory T cells (T_{regs}) in human lower grade BRAF-altered glioma, as compared to BRAF wildtype astrocytoma [89]. The effects of BRAFi+MEKi on the tumor immune infiltrate has yet to be assessed.

In contrast to other models previously generated our orthotopic mouse model is fully immune competent. Thus, we assessed the presence of T cells and inhibitory immune checkpoints in BRAF V600E-mutated gliomas in our syngeneic orthotopic murine BRaf V600E Ink-/- gliomas by immunofluorescence. Staining for T cell markers and the cytotoxic T-lymphocyte antigen-4 (CTLA-4), a second important inhibitory immune checkpoint, and PD-L1 revealed that effector T cells (CD4+, CD8+) and CD4+Foxp3+ regulatory T cells (T_{regs}), as well as CTLA-4+ cells and PDL-1+ cells are present within the tumor mass. CTLA-4 was expressed on CD8+ and CD4+ T cells as expected (**Figs. 6A and 6B**), while PD-L1 was expressed on both Nestin+ and Nestin- cells **(Figs. 6D and 6E)**. The presence of PD-L1 was confirmed in patient tissue derived from BRAF V600E-mutated CDKN2A-deleted high-grade astrocytoma **(Figs. 6G and S6A; Table 1)**.

These data indicated that our murine orthotopic tumor model harbors an T cell immune infiltrate with T cells and tumor cells expressing T cell inhibitory signals.

Concurrent MAPK pathway inhibition combined with inhibitory immune checkpoint blockade enhanced antitumor efficacy in a T-cell-dependent manner

T cell activation triggers upregulation of immune inhibitory checkpoints. Therapeutic antibodies release the inhibitory checkpoints and re-activate T cells. The effects of combining BRAFi+MEKi treatment with immune checkpoint blocking antibodies was assessed in our syngeneic orthotopic murine BRaf VE Ink-/- gliomas using high-dimensional single-cell mass cytometry (CyTOF). Orthotopic tumor-bearing mice were treated concurrently with dabrafenib and trametinib (BRAFi+MEKi) alone [42], and in combination with anti-PD-1 or anti-PD-L1, combined with anti-CTLA-4 antibodies, for 14 consecutive days **(Fig. 7A)**. CyTOF analyses gated on viable T cells revealed an increase in the frequency of intra-tumoral CD4+ and CD8+ T cells upon concurrent treatment with Dabrafenib and Trametinib *in vivo* **(Figs. S7A)**. The frequency of T cells expressing immune checkpoint inhibitory molecules (PD-1+CD8+ and PD-1+CD4+, CTLA-4+CD8+ and CTLA-4CD4+) T cells was significantly increased with BRAFi+MEKi treatment, as visualized by nonlinear dimensionality reduction (t-SNE). As expected, therapeutic antibodies alone or the quadruple treatment (BRAFi+MEKi+anti-PD-1/anti-PD-L1+anti-CTLA-4) counteracted this increase in inhibited T cells (**Figs. 7C and 7D**). Similar data were obtained when anti-PD-L1 antibody was used instead of anti-PD-1 antibody (data not shown). These data corroborated the RNAseq data obtained with BRAFi+MEKi-treated cells *in vitro* and suggest that T cells are activated with BRAFi+MEKi and express inhibitory signals. We corroborated the increase in T cells expressing inhibitory signals in response to BRAFi+MEKi by immunofluorescence **(Figs. S7C and 7D).** Adding therapeutic antibodies (anti-PD-L1+α-CTLA-4) to BRAFi+MEKi treatment decreased PD1+ and CTLA4+T cells. Combined quadruple

treatment showed greater efficacy against CD4+CTLA4+ T cells when compared with single α-PD-1 treatment (**Figs. 7C and 7D**).

We tested next whether concurrent treatment with therapeutic antibodies (α-PD-L1+ α-CTLA-4) and pharmacological BRAFi+MEKi have an additional survival benefit, as suggested by our CyTOF data. Concurrent dabrafenib and trametinib treatment significantly extended the survival of mice subjects bearing orthotopic BRaf VE Ink-/- glioma-bearing compared with vehicle-treated control mice, consistent with our previous study [42]. Similar survival benefits were seen with concurrent anti-PD-L1+anti-CTLA-4 therapies alone. Continuous, and concurrent BRAFi+MEKi and ICI provided an additional survival benefit, extending survival by 114% when compared to BRAFi+MEKi alone. Interestingly, the survival benefits of therapeutic antibodies alone and synergistic effects were completely abolished in athymic mice; this is indicative of T cell-mediated anti-tumor efficacy by therapeutic antibodies **(Figs. 7E, 7F).**

DISCUSSION

Chemotherapy is the standard of care for low-grade gliomas, with radiotherapy generally reserved as a treatment for progressive cases [90-92]. Molecular targeted therapies have revolutionized the treatment of brain tumors that respond poorly to chemotherapies, and these include BRAF V600E mutated brain tumors, which are an important clinical paradigm for molecular targeted treatment with BRAF and MEK inhibitors responses; despite these novel therapies, these tumors frequently progress and fail to respond to treatment. Novel therapeutic approaches are necessary to overcome tumor rebound and therapy resistance, which is especially common in high-grade gliomas. Experimental therapeutics depend on mouse models that closely resemble the human diseases and these are scarce in particular for gliomas. This study presents a novel mouse model for BRAF

V600E mutated gliomas that closely simulates the genetic alterations of low-grade tumors at high risk for progression and high-grade gliomas. Several models of BRAF V600E mutated gliomas (both low- and high-grade) have been generated and have provided important insights into tumor development [41, 42, 75, 93]. Previous mouse model studies were geared towards testing the cooperativity of constitutively active BRAF with genetic alterations that coincide with BRAF V600E in human cancer [41, 42, 68, 94]. In past models, it has been demonstrated that BRAF V600E expression in mouse brain cells induces formation of high-grade gliomas only when combined with additional oncogenic alterations; these can include activated Akt, loss of tumor suppressors Tp53, or loss of tumor suppressor locus Ink4a/Arf, the mouse homolog of the *CDKN2A* locus [41, 68]. For the current model we also combined BRAF V600E expression with CDKN2A deletion, as we have investigated previously [41], and as expected we observed formation of high-grade tumors. The most frequent neuroanatomical origin of human BRAF V600E mutated high-grade gliomas [41, 95] in the cerebral hemispheres [6], and so our model appropriately reflects a defined neuro-anatomical origin of the human tumor [23, 55, 56]; this is in contrast to previous models that were generated agnostically to the tumor location. Our model also differs from many other previous models: rather than driving exogenous expression of BRAF V600E from a viral vector or as in a more recent study by a transposon [75, 93] it uses a Cre-activatable transgenic knock-in allele of BRAF V600E. In our model, expression of the mutant kinase was induced by expression of Cre, and the expression levels of the mutant gene are controlled by the endogenous BRAF promoter, which allowed us to better mimic the expression in the human disease. The cortical areas targeted by adenovirus-Cre expression are reportedly devoid of neural stem cells in mice, which supports a non-stem cell origin of our murine BRAF V600E mutated high-grade gliomas. A limitation of our model is that Cre expression was

introduced by injection of adenovirus-Cre which contains a ubiquitous promoter, and therefore we could not determine the cell type of origin of our murine BRAF mutated high-grade gliomas. Reactive astrocytes and resident OPCs are concentrated at the tumor periphery of our murine BRaf V600E-mutated gliomas, and the latter potentially have a barrier function for invasion into striatal areas. This observation warrants future investigations into the roles for OPCs in tumor development. Lastly, existing preclinical models of BRAF V600E mutated glioma are immune compromised and therefore prohibitive for testing immune therapies that have revolutionized cancer treatment. Here, we have generated a fully immune competent mouse model that can be applied for preclinical testing of immunotherapies. Thus, our new model recapitulates the genetic and neuroanatomical aspects of BRAF V600E mutated human gliomas in the presence of a complete immune system.

Physiological MAPK signaling plays multiple roles in the mammalian brain, including in glial cell differentiation. A genetically engineered knock-out of B-Raf in mice impairs oligodendrocyte differentiation [96]. BRAF V600E expression diverts cell fate from neuronal to glial lineage and impairs differentiation of mouse embryonic neural stem cells [41, 97]. We found that expression of BRAF V600E in murine adult neural stem cells increased the frequency of oligodendrocyte progenitor cells (OPCs) by inducing symmetric divisions and impaired differentiation; this is a similar observation to a previous study in adult oligodendroglioma [79]. Our data suggest that BRaf V600E expression combined with CDKN2A deletion mainly promotes proliferation of cells resembling oligodendrocyte lineage cells. Interestingly, BRAF V600E expression did not alter CD133+ cell frequency and asymmetric divisions, suggesting diverse responses to MAPK signaling activation. Our data in murine BRAF V600E mutant gliomas rather suggest that

oncogene expression increased intra-tumoral cellular heterogeneity, by differentially expanding immature progenitor-like cells (but not CD133+ cells).

We showed that in addition to well-documented cytostatic and cytotoxic effects of BRAF and MEK inhibitors, they also reverted oncogene-induced OPC defects in asymmetric divisions and differentiation; this indicated that clinically relevant MAPK pathway inhibitor treatment alters the differentiation states of human BRAF V600E mutated glioma cells, which is important since OPC-like tumor cells play important roles in tumor origin and proliferation.

Molecular and phenotypic intratumoral heterogeneity has confounded attempts to inhibit individual actionable targets in gliomas, this heterogeneity contributes to therapy resistance and the poor prognosis of glioma patients, despite aggressive standard adjuvant therapy [98-100]. Genomic feature-based deconvoluting algorithms have inferred that an average of four genetically distinct clones coexist in solid cancers at biopsy or surgery with the numbers and sizes of clones varying amongst cancer types [101, 102]. Recent advances in single cell sequencing have further revealed that these genetically defined clones comprise functionally and phenotypically distinct tumor cell subpopulations representing distinct cellular states [78, 103-105]. Immunophenotyping and single cell analyses suggested that BRAF V600E-mutated gliomas, like other solid cancers exhibit substantial intratumor heterogeneity (ITH) [40, 78]. Heterogenous tumor cells respond differently to BRAF inhibition [30, 101, 102], and our recent data indicated that elevated polo-like-kinase 1 (Plk1) activity in tumor subpopulations marked by CD133 expression contribute to resistance to BRAF inhibitor treatment [40]. Our adenovirus-Cre-induced mouse model recapitulated some of the phenotypic heterogeneity predicted of human BRAF-mutated gliomas [40, 78, 106, 107], expressing a wide range of neural stem and progenitor cell and to a lesser extent differentiated glial cell markers. Finding that *CD133* mRNA and CD133 protein are present in

treatment-naïve BRAF V600E mutated murine glioma corroborated our earlier reported data in human samples [40]. This study shows that levels of *CD133* mRNA and CD133 protein are heightened in a patient's recurrent BRAF V600E-mutated glioma following treatment with BRAFi/MEKi combination therapies. Combined with earlier findings that human CD133+ subpopulations responded less to the anti-proliferative effects of BRAF inhibitor when compared with the tumor bulk [40], our data in the murine model and novel patient-derived cells suggested that CD133 expression marks a therapy-resistant compartment that is not only conveying resistance to conventional chemoradiotherapy [81] [108] but also contributes to resistance to molecular targeted inhibition of MAPK pathway signaling. Collectively, our data showed that oncogene expression disrupts asymmetric distribution of NG2, consistent with an increase in NG2+ glioma cells. CD133+/Prom1+ glioma cells are not as sensitive to BRaf V600E expression and pharmacological BRAF V600E inhibition. Lastly, CD133+ cells negative for Nestin were detected after BRAFi+MEKi treatment *in vivo*. This CD133+ subpopulation appears to be a novel population that downregulates Nestin expression in response to BRAFi+MEKi.

The pentaspan transmembrane glycoprotein CD133 is expressed on hematopoietic [109, 110], human neural stem cells [111], and more differentiated cells [74] and cancer stem cells (CSC). Due to their increased ability for DNA repair [81, 82], mesenchymal transition [112], metabolic adaptation [113], and slow and asymmetric proliferation modes [114-116], CSCs are thought to survive standard chemoradiation better than non-stem-like cells; they are therefore potential culprits for therapy resistance and recurrence in multiple human cancers [117-119], such as leukemia [120], pancreatic cancer [121], colon cancer [122], and brain tumors [123]. Recent reports suggest that CD133 is a prognostic marker for relapse [124, 125], and independent risk factor for progression and marker for poor clinical outcome in glioma patients [126, 127], further

underscoring the clinical importance of this marker. While we do not yet know the significance of CD133 expression in BRAF V600E-mutated high-grade gliomas and the function of CD133+ cells, these findings are relevant given that many patients are stratified to receive targeted therapies in the clinic and frequently develop resistance to such treatments.

The overall response rates (ORR) to Dabrafenib + Trametinib was 62% in low-grade and 29% in high-grade glioma patients, indicating that tumor cells escape from dual MAPK pathway inhibition. Multiple studies have demonstrated mechanisms for resistance to BRAFi+MEKi in non-CNS BRAF-mutant solid cancers, including genetic mutation events in the MAPK and PI3K pathways, and purely transcriptomic events based on changes in DNA methylation [27, 128-130]. Mechanisms of resistance for BRAF inhibitor in patient samples and xenografts, are poorly understood and have only recently been investigated [40, 42, 45]. . Reported resistance mechanisms include loss of NF1, PTEN, and CBL [131].

Similarly much less is known about the immune modulatory effects of BRAFi+MEKi in glioma versus other solid tumors. The BRAF-MEK signaling pathway and BRAF V600E mutation governs immune evasion [58-60], whereas BRAF and MEK inhibition increased immune-based anti-tumor effects in melanoma [61-66]. BRAF and MEK inhibitors profoundly alter the tumor immune infiltrate in metastatic melanoma [61, 62, 84-86], by improving melanoma antigen presentation and enhancing the immune response [61, 132]. Moreover, transcriptional changes associated with resistance to MAPK pathway inhibition in melanoma involve genes and pathways associated with migration of immune cells and inflammatory tumor infiltration [133].

In chronic inflammatory conditions such as cancer, prolonged T cell activation leads to upregulation of immune checkpoint molecule CTLA-4 on cytotoxic T cells and an increase in T

regulatory (Treg) cells, both known to reduce T cell numbers [134]. In gliomas, the T cells are further inhibited, and the immune suppressive phenotypes are strengthened by expression of immune checkpoint molecule programmed death-ligand 1 (PD-L1) on tumor cells and the circulating macrophages/monocytes [135, 136]. The increased frequency of PD-1 and CTLA-4 positive cells upon dual MAPK pathway inhibition are therefore indicative of an anti-tumor immune response followed by a dysfunctional state of T cells likely due to prolonged MHC antigen presentation induced by BRAFi+MEKi treatment.

Dual MAPK pathway inhibition (MAPKi) by Dabrafenib+Trametinib, Vemurafenib+Cobimetinib, Encorafenib+Binimetinib, and immune checkpoint inhibition (ICI) by nivolumab (anti-PD-1) and nivolumab/ipilimumab (anti-PD-1/anti-CTLA-4) combination have revolutionized the treatment of BRAF V600E-mutated advanced melanoma. Despite encouraging data in mouse models [137-143], immune checkpoint blockade with therapeutic antibodies against PD-1/PD-L1 failed to demonstrate a significant benefit in glioblastoma. Elevated CD3+CD8+ T cell frequency correlates with improved patient survival in GBM [149], while regulatory T cells (T_{reg}) reportedly mediate immune escape by suppressing T cell activity [150]. The lack of T cell infiltration and immune activation are thought to contribute to a general immunologically “cold” phenotype [101, 144] and could explain the lack of efficacy in gliomas [145]. Pediatric gliomas are inherently classified as tumors of low immunogenicity by emerging immunogenomic analyses [146], in part because they lack an active T cell infiltrate [151]. This is in part because pediatric tumors typically carry lower numbers of nonsynonymous somatic mutations when compared with adult tumors of the same histology [147], although the relationship between tumor mutation burden and response to cancer immunotherapy has recently been challenged in recurrent glioblastoma [148].

BRAF V600E-mutated gliomas could be an exception: recent data showed that CD8+ T cells are increased while Treg cells are decreased in human BRAF-altered gliomas compared with BRAF-wildtype, IDH1- mutated control gliomas [89]. These data are in line with earlier studies showing that high-grade tumors with a PXA methylation profile, which include BRAF V600E-mutated gliomas, exhibit upregulated cytokine signaling, and cell junction organization programs and a significantly higher frequency of CD8+ tumor-infiltrating lymphocytes compared with non-PXA high-grade glioma subtypes [55, 56]. Methylation, histopathological, and molecular analyses recently subdivided BRAF V600E CDKN2A deleted gliomas further according to their LUMP score, which is a surrogate marker for leukocyte/lymphocyte infiltration [69].

Active T cell infiltration in our murine glioma model corroborates the above mentioned data in human patients. Immune checkpoint inhibition (ICI) reduces T cell activation, and thus is a mechanism exploited by tumors to escape from T cell recognition and immune mediated elimination [134]. Our discovery that BRAF V600E-mutated human gliomas express PD-L1 – the inhibitory immune checkpoint molecule known to dampen the anti-tumor immune response - could explain why BRAF V600E mutated low-grade tumors have a poorer prognosis than their BRAF wildtype counterparts despite their higher levels of T cell infiltration.

Monoclonal antibodies (such as pembrolizumab and nivolumab) against programmed cell death proteins (PD-1) on T cells, as well as the ipilimumab against cytotoxic T lymphocyte antigen-4 (CTLA-4), are immune checkpoint inhibitors which restore a suppressed T cell anti-tumor response. These therapeutics are FDA-approved for melanoma and other solid cancers [31] and have seemingly similar efficacy profiles as BRAFi+MEKi in advanced melanoma harboring a BRAF V600E advanced melanoma. This complicates therapeutic decision-making and leaves many open questions about the optimal sequence and potential combinations therapies.

MHC molecules are strongly associated with a state of immune sensitization [152]. Our data showing upregulation of MHC class I and class II genes in response to BRAFi+MEKi indicate that these therapies increased the neoantigen load. Abundant PD-L1+ tumor-associated macrophages and lack of MHC-II-expressing antigen-presenting cells are associated with resistance to dual CTLA-4/PD-1 checkpoint blockade in glioblastoma patients [153]; this suggested that poor antigen presentation contributes to failure of immunotherapy of high-grade glioma. Persistent antigen exposure on the other hand profoundly contributes to T cell dysfunction, which is corroborated by an increase in T cells expressing inhibitor checkpoints in our study. This leads to tumor immune escape in glioma [154]. Single-agent PD-1 blockade failed to demonstrate a survival benefit in recurrent glioblastoma [155], and only a few objective responses were observed with pembrolizumab in the compassionate use setting [101, 144, 145, 155]; this prompted clinical assessment of multiple therapeutic immune checkpoint inhibitory agents, based on effective strategies in other malignancies. While many agents remain under clinical observations, profiling of glioma patients identified a dominant immunosuppressive axis refractory to immune function restoration [156]. Retrospective analyses found that only subsets of patients could benefit from combined PD-1/CTLA-4 blockade.

Our preclinical data show that concurrent inhibition of the PD-L1/PD1 and CTLA-4 checkpoints, which affect T cell functions non-redundantly, overcomes T cell dysfunction and reduces tumor growths more effectively than BRAFi+MEKi alone. This supports the hypothesis that BRAF V600E-mutated gliomas could potentially be susceptible immune checkpoint inhibition (ICI) therapies [55, 56]. Given the elevated toxicities with dual ICI over single ICI, future studies should aim to determine if single-agent checkpoint inhibitors are efficacious in combination with BRAFi+MEKi [157].

MATERIALS AND METHODS

In vivo Animal Studies

For mouse studies male and female mice were used. All animal procedures were performed in accordance with institutional and federal guidelines (Stanford University APLAC protocol #33633). Compound transgenic mice were generated by combining the Cre-conditional allele of BRAFV600E, BRAF CA [71] with Ink4a/Arf flox/flox [72] mice. Two different Cre reporters were used, the tdTomato reporter (B6.Cg-Gt(ROSA)26Sor tm14(CAG-tdTomato)Hze/J) and the ROSA26 Cre reporter strain [158]. BRAF CA/WT Ink4a/Arf flox/flox mice were of a pure FVB/N genetic background. Littermates carrying appropriate genotype(s) were randomly assigned to experimental groups. Pure FVB/N mice (Jackson Laboratory) were intracranially injected at 6-8 weeks of age. Mice were treated and analyzed, as indicated in the text and figure captions.

Human Studies

Tumor specimens and clinical information were collected according to the Stanford IRB protocol approved by the Research Ethics Board. Patients provided informed consent, and ethical approval was obtained from the Institutional Review Board at Stanford University. Permanent fixed brain tumor tissue was obtained from patients with BRAF/RAF/MAPK mutations with CDKN2A loss and IDH-mutant astrocytoma. Clinically relevant dual MAPK pathway inhibitors were administrated to a 13-yr-old boy with BRAF-mutant high-grade glioma. The patient was initially treated with one cycle of doxorubicin/ifosfamide treatment with 65.20 Gy in 35 fractions radiotherapy, and subsequently underwent Dabrafenib plus Trametinib treatment.

Cell Lines and Primary Cultures

All cell lines and primary cultures were maintained in humidified cell culture incubators at 37°C under 5% CO_2. SU-aGBM5 is a BRAF V600E mutant GBM cell line from a young adult obtained from Dr Michelle Monje (Stanford University, CA, USA) [159]. Murine BRAF V600E mutant glioma cell lines were derived from murine glioma, induced by injection of adenovirus-Cre into the brain of BRAF $^{CA/WT}$ Ink4a/Arf $^{flox/flox}$ mice, as previously described [41, 42]. Murine neurosphere cells were generated by adenovirus-cre infection of cells isolated from the corpus callosum of young adult BRaf $^{CA/WT}$ Ink4a/Arf $^{flox/flox}$ and BRaf $^{WT/WT}$ Ink4a/Arf $^{flox/flox}$ brains. Authentication of the patient-derived cell line was performed by whole exome sequencing and qRT-PCR.

Intracranial Injections of Adenovirus

BRaf $^{CA/WT}$ Ink4a/Arf $^{flox/flox}$ mice were injected with 2 uL (10^9 multiplicity of infection (MOI)) of adenovirus expressing cre recombinase under the control of the ubiquitous CMV promoter (Ad-Cre; Vector Biolabs) to induce BRaf V600E expression and deletion of tumor suppressor genes p16 ^{Ink} and p19 ^{Arf} [41]. Control mice were injected with adenovirus expressing GFP (Ad-GFP; Vector Biolabs). Specific coordinates listed in Figure S1C were selected to target two different cortical layers. Animals were sacrificed at specific timepoints post-virus injection, as indicated in the text, to detect virus-infected cells (4-days post injection) and premalignant lesions (21-days post injection). Remaining mice were observed and sacrificed when exhibiting neurological symptoms consistent with intracranial tumor formation. Brains of symptomatic mice were resected, sectioned and tumor-bearing brains were subjected to hematoxylin and eosin (H&E), X-Gal staining, and immunofluorescence staining.

Immunohistochemistry, Enzymatic and Immunofluorescence Stainings

Mice were perfused by cardiac puncture with phosphate buffered saline followed by 4% paraformaldehyde (PFA), brains were resected, post-fixed overnight and either cryoprotected in sucrose (15% day-1 post-perfusion, 30% day-2 post-perfusion) and embedded in OCT (TissueTek, Sakura) or dehydrated and embedded in paraffin.

Immunofluorescence on frozen tissue sections

Frozen 10-15 um sections were placed on Superfrost slides, post-fixed for 10 min at room temperature with 3.7% PFA, washed briefly in PBS, blocked in the appropriate blocking agent in 0.1% Triton-X-100 and PBS for 1 hr. at room temperature. Sections were incubated with primary antibodies overnight at 4^{o}C in a humidified chamber, washed briefly in PBS, incubated with fluorophore-conjugated secondary antibodies in blocking buffer for 1hr. at room temperature, washed briefly in PBS, and mounted in a DAPI-containing mounting solution (VectaShield or Southern Biotech). Primary antibodies used were guinea pig or rabbit anti-NG2 (Millipore), rabbit Olig2, rabbit anti-beta-galactosidase (Abcam), chicken anti-Nestin (Abcam), rat anti-GFAP (Thermo Fisher Scientific), rabbit anti-Ki67 (Abcam), rat anti-CD133 (Thermo Fisher Scientific), rat anti-MBP (Abcam), rat anti-CD8 (BioLegend), rat anti-CD4 (BioLegend).

Differentiation assays

Differentiation assays were performed as previously published [79, 160] with minor modifications. Dissociated cells were plated on Lab TekII coverslips pre-coated with 10 ug/ml laminin or on

round glass coverslips pre-coated with 0.01% poly-l-lysine for two days in proliferation media, followed by 5 days in 2% fetal bovine serum (FBS) for undirected differentiation or 2% FBS with growth factors (EGF, bFGF, PDGFAA, PDGFBB), or 10 days in 60 nM triiodothyronine (T3, Sigma), 100 ng/mL insulin-like growth factor-1 (IGF-1, Shenandoah), and 10 ng/mL CNTF (Peprotech) with fresh media added every 3 days, for promoting oligodendrocyte or astrocyte differentiation. Cells were fixed with 3.7% PFA (EMD) for 10 min at RT and stained with primary antibodies overnight and fluorophore-conjugated secondary antibodies for 1hr. before being mounted in VectaMount. Images were collected on a Zeiss LSM700 confocal microscope and processed for cellular quantitative analysis using Fiji.

5-ethynyl-2'-deoxyuridine (EdU) incorporation

Tissue sections were fixed in 3.7% PFA in PBS, followed by permeabilization with 0.5% Triton-X-100 for 20 minutes. Sections were incubated with 1 X Click-iT buffer additive diluted in deionized water and Click-iT reaction cocktail according to the manufacturers' protocol (Invitrogen, C10337) for 30 min at room temperature protected from light. Imaging was performed at the Axioscope (Zeiss).

Flow Cytometry, mass cytometry, FACS, MACS

For flow cytometric analyses of CD133+ and NG2+ cell frequency, neurosphere cultures were dissociated using PBS (Ca2+, Mg2+-free) + 0.2 mmol/L EDTA, resuspended in FACS buffer (PBS+EDTA+0.5% BSA) at 1E6 cells/100 uL, and incubated with primary antibodies: Prom1 (Miltenyi Biotec, Clone MB93G8), NG2 (Millipore, ab5320). Isotype IgG and single channel

antibodies were used as a control. Cells were washed, secondary antibodies were added if appropriate, and cells were resuspended in a FACS buffer containing Hoechst and strained immediately prior to analyses. Cells were analyzed by flow cytometry using the FACS Calibur and cell sorting was performed using a BD Biosciences ARIA 3 cytometer. Raw data was processed and analyzed with the FlowJo software (10.7.1).

BRaf VE Ink -/- orthotopic glioma-bearing mice were treated with vehicle or D+T for 3 days. Collagenase was used for tumor cell dissociation, and A2B5+ cells were selected from the dissociated tumors using magnetic cell isolation methods (Miltenyi). Total RNA isolated from the sorted cells was used for subsequent RNA-seq experiments.

For CyTOF mass cytometry, orthotopic tumors were resected from perfused brains, and digested with a mix of collagenases and DNAse. Single cell dissociates were fixed and analyzed by mass cytometry, as described [153]. Raw mass cytometry data were imported into CytoBank, and further analyzed downstream by FlowSOM.

cDNA Synthesis and Quantitative PCR

Total RNA was extracted using the RNeasy Plus kit (QIAGEN) and cDNA synthesis was performed using the iScript cDNA Synthesis Kit (Biorad). Quantitative RT-PCR was run using SYBR Green PCR Master Mix (Thermo Fisher Scientific) using a cycling program of 10 min at 95^{o}C followed by 40 cycles of 95^{o}C for 15 sec and 95^{o}C for 60 sec. All primer sequences are available in Table S3.

RNA Sequencing and Analysis

RNA concentration was quantified by Nanodrop (Nanodrop Technologies, Wilmington, DE) and 0.4 ug of each sample were submitted to Novogene (Novogene Corporation Inc., Sacramento, CA) for RNA sample QC, library preparation, Sequencing (Illumina PE150, 20M paired reads). FASTQ files were uploaded to Galaxy (usegalaxy.org), an open source, web-based platform for sequencing analysis where we performed quality control (FastQC), mapped the reads to the human or mouse genome (STAR aligner), counted reads per annotated gene (FeatureCounts), and determined differentially expressed features (DESeq2). Pathway enrichment analysis was performed using gene set enrichment analysis (GSEA) combined with pathway definitions from MSigDB, KEGG and Reactome databases. GSEA was run using pre-ranked mode for all genes based on log2 fold change derived from the differential expression analysis. Pathways with a normalized enrichment score >1 or <-1 at FDR <10% were considered significant. RNA sequencing data are available in Tables S1 and S2.

Quantification and statistical analysis

All experiments were performed in duplicate (RNA-seq experiment) or triplicates (immunocytochemistry, flow cytometry, qRT-PCR). Between five and eight mice were assigned to each study arm (untreated, treated, injected in CXI, injected in CXII). Data are presented as mean ± SEM. All statistical analyses except for RNA seq were conducted using GraphPad Prism software (version 8.3.0, GraphPad Software, San Diego, California USA, www.graphpad.com). A P value less than 0.05 was used to determine statistically significant differences.

If not otherwise indicated in the text, a Mann Whitney T test and Multiple unpaired t tests were performed for quantifications of immunofluorescence data for T cells and tumor cells whenever 2 conditions (untreated and inhibitor treated samples were compared). An ordinary one-way

ANOVA and Tukey's multiple comparisons test were performed when multiple comparisons were made. Survival curve comparison was performed using a Log-rank (Mantel-Cox) test (conservative).

Figure Legends

Figure 1:

(A) Top: Schematic of a coronal view of a mouse brain indicating the neuroanatomic injection for adenovirus expressing cre recombinase (Ad:Cre) into BRaf CA/WT Ink4a/Arf flox/flox mice or control mice. CX=cortex. Bottom: Survival curves of BRaf CA/WT Ink4a/Arf flox/flox mice injected with Ad:Cre into inner (CX I), and outer (CX II) cortex or Ad:GFP, as a control.

(B) Top: Representative X-Gal and hematoxylin- double-stained brain tissue section at 4 days post-injection (p.i.) with Ad:Cre into the inner cortex, showing beta-galactosidase-positive cells (arrow) adjacent to the injection track (asterisk) at low (left) and high (right) magnification. Scale bars, 2 mm (left), and 200 μm (right).

Bottom: Representative H&E-stained brain tissue section of endogenous BRaf CA/WT Ink4a/Arf flox/flox (=BRaf CA Ink Lox/Lox) mouse injected with Ad:Cre into the inner cortex, at endpoint, showing diffuse growth of a malignant astrocytoma-like tumor in the adjacent corpus callosum and cortex at low (left), and high (right) magnification. Scale bars, 1 mm (left), and 100 μm (right).

(C) Representative co-immunofluorescence staining of endogenous BRaf V600E mutated CDKN2A deleted endpoint tumors for beta-galactosidase (bGal), GFAP, and DAPI for DNA. Scale bar, 200 μm

(D) Representative co-immunofluorescence staining of endogenous BRaf V600E mutated CDKN2A deleted endpoint tumors for Nestin, GFAP, and Olig2. Scale bar, 50 μm

(E) Representative co-immunofluorescence staining of endogenous BRaf V600E mutated CDKN2A deleted endpoint tumors for NG2, phospho-ERK (p-ERK), and KI67. Scale bar, 50 μm

(F) Representative co-immunofluorescence staining of BRaf V600E mutated CDKN2A deleted orthotopic gliomas at endpoint for GFP and NG2. Scale bar, 100 μm

(G) Representative co-immunofluorescence staining of BRaf V600E mutated CDKN2A deleted orthotopic gliomas three weeks post-injection for proliferation marker Ki67 with Olig2 at low (top) and high (bottom) magnification. Scale bar, 200 μm (top) 50 μm (bottom).

(H) CD133/Prom1 of BRAF V600E mutated CDKN2A orthotopic tumors. Bottom panels are high magnification images. Scale bars, 100 μm (top), 10 μm (bottom).

Quantification of the data shown in (G) and (H) revealed that the percentage of CD133/Prom1-positive cells amongst Ki67-positive cells was significantly lower than that of Olig2-positive cells. An unpaired t test was performed to compare the two populations. The P value is ****<0.0001. The mean of Olig2+ cells amongst Ki67+ cells = 64.4 percent; the mean of CD133/Prom1+ cells amongst Ki67+ cells is 19.4 percent.

Five individual tumors were counted.

Figure 2:

(A) Left: Representative flow cytometry plot for oligodendrocyte progenitor cell marker NG2- and CD133/Prom1-positive single cells sorted from BRaf wildtype (WT) CDKN2A deleted and BRaf V600E mutated CDKN2A deleted neurospheres grown under proliferative conditions. Right: Graph shows quantification of flow cytometry analyses for NG2-positive, CD133/Prom1-positive or other cells.

(B) BRaf WT CDKN2A deleted and BRaf V600E mutated CDKN2A deleted cells were plated in undirected differentiation medium and subjected to immunofluorescence for A2B5 and Nestin. Scale bar = 20 µm.

(C) Quantification of immunofluorescence for neural progenitor marker Nestin and A2B5 in BRaf WT CDKN2A deleted and BRaf V600E mutated CDKN2A deleted cells plated in undirected differentiation media. **p<0.01; ***p<0.001

(D) Representative images of immunocytochemistry staining for OPC marker NG2 and mature oligodendrocyte marker myelin basic protein (MBP) of BRaf WT CDKN2A deleted and BRaf V600E mutated CDKN2A deleted neurosphere cells. These cells were kept for 10 days in oligodendrocyte-promoting differentiation media containing IGF-1 and T3. Scale bar, 20 µm.

(E) Quantification of (D). Data are shown as mean ± SEM of at least 3 independent experiments. **P < 0.01; ***P < 0.001 as assessed by unpaired t-test.

(F) Representative images of immunocytochemistry staining for OPC marker NG2 and DAPI for DNA of BRaf V600E mutated CDKN2A deleted glioma cells. The cells were kept for

5 days in media containing 2 % fetal bovine serum with or without growth factors and were treated with 1nM dabrafenib and trametinib. Scale bar, 80 μm.

(G) Quantification of (F)

(H) Representative images of immunocytochemistry staining for mature astrocyte marker GFAP, neural progenitor cell marker Nestin, and DAPI for DNA of BRaf V600E mutated CDKN2A deleted glioma cells. The cells were kept for 5 days in media containing 2 % fetal bovine serum with or without growth factors and were treated with 1nM dabrafenib and trametinib. Scale bar, 90 μm.

(I) Quantification of (H). Data are shown as mean ± SEM of at least 3 independent experiments. *P < 0.05; **P < 0.01; ***P < 0.001 as assessed by unpaired t-test.

(J) Expression levels of the individual samples for the genes of interest including *cspg4, cnp, cldn11, mbp, gfap, aldoc* and *nes*. *P < 0.05 as assessed by differential gene expression analysis with DESeq2.

Figure 3:

(A) Top: Representative asymmetric cell division in BRaf WT CDKN2A deleted (Ink-/-) cells showing a cell pair with NG2 in just one of the two opposing daughter cells; next to a representative symmetric cell division in BRaf V600E mutated CDKN2A deleted cells showing a cell pair with NG2 in both opposing daughter cells; scale bar, 50 μM. Bottom: Representative asymmetric cell divisions in BRaf WT CDKN2A deleted (Ink-/-) and BRaf V600E mutated CDKN2A deleted cells showing cell pairs with CD133/Prom1 in just one of the two opposing daughter cells.

(B) Quantification of asymmetric protein distribution in percentage of WT. *P<0.01 as assessed by two-way ANOVA.

(C) Representative asymmetric cell divisions in BRaf V600E mutated CDKN2A deleted glioma cells showing cell pairs with NG2 in just one of the two opposing daughter cells in control-treated and BRAFi+MEKi-treated conditions: scale bar, 50 uM.

(D) Quantification of asymmetric protein distribution in percentage of control-treated conditions.

(E) Schematic of treatment regimen of syngeneic mice carrying orthotopic BRAF V600E mutated CDKN2A deleted gliomas with dabrafenib (BRAFi/D; 2.5 mg/kg i.p. daily), and trametinib (MEKi/T; 1 mg/kg p.o. daily). Vehicle treatment with DMSO was used as control and treatment lasted five days.

(F) Flow cytometry analysis of CD133 and Nestin expression among BRAF V600E mutated CDKN2A deleted glioma cells treated with vehicle control (DMSO, left) or BRAFi + MEKi (right). P1 indicates cells positive for both CD133 and Nestin. P2 indicates cells positive for CD133 only.

(G) Quantification of flow cytometry analysis in (H). ***P<0.001 as assessed by unpaired t-test

(H) Representative co-immunofluorescence staining of BRaf V600E mutated CDKN2A deleted orthotopic gliomas at endpoint for Nestin, CD133/Prom1, and DAPI for DNA; Scale bar, 50 μm

Figure 4:

(A) Magnetic resonance images (MRI) from a BRAF V600E mutated high-grade glioma in the parieto-occipital region at the treatment-naïve stage (Day 0), post-resection (Day 1), and after extensive treatment with chemotherapy, and BRAF inhibitor dabrafenib plus MEK inhibitor trametinib.

(B) Hematoxylin & Eosin (H&E) staining of the resected tumor prior to systemic treatment and post-treatment (at autopsy).

(C) Representative immunohistochemistry for CD133 in a treatment-naïve tumor and post-treatment (at autopsy) at low (left) and high magnification (right). Scale bars, 100 μm (left); 50 μm (right).

(D) Quantification of CD133+ cells in five tumor fields.

(E) *CD133* mRNA expression in treatment-naive cells and cells from tumor after treatment and recurrence. Cells were incubated with DMSO (vehicle control) or concurrently with BRAFi dabrafenib (D) and MEKi trametinib (T) for 48 hr. The expression of *CD133* mRNA as determined by qRT-PCR. Data shown as mean ± SD of at least 3 independent experiments. **P < 0.01; ***P < 0.001 as assessed by unpaired t-test; n.s.=not significant.

(F) *CD133* mRNA expression in BRAF V600E mutated established glioblastoma cell lines (DBTRG; AM38) and a patient-derived cell line (SU-aGBM5) incubated with DMSO (vehicle control/Ctrl) or concurrently with BRAFi dabrafenib (D) and MEKi trametinib (T) for 48 hr. The expression of *CD133* mRNA as determined by qRT-PCR. Data shown as mean ± SD of at least 3 independent experiments. *P < 0.05; **P < 0.01; as assessed by unpaired t-test.

(G) Viability of treatment-naive cells and cells from tumor after treatment and recurrence. Cells were incubated with DMSO (vehicle control) or concurrently with BRAFi dabrafenib (D) and MEKi trametinib (T) for 48 hr. Cell viability was determined by an Alamar Blue viability assay. Data shown as mean ± SD of at least 3 independent experiments. ****P < 0.0001 as assessed by unpaired t-test; n.s.=not significant.

Figure 5:

(A) Two-sided bar charts illustrating the normalized enrichment score of gene set Enrichment analysis (GSEA) of *ex vivo* isolated cells from BRAF V600E mutated CDKN2A deleted murine glioma-bearing brains (419), treated concurrently with BRAFi (dabrafenib) + MEKi (trametinib) or vehicle.

(B) GSEA enrichment plot of *ex vivo* isolated cells treated with BRAFi + MEKi versus vehicle. The peak in the plot indicates upregulation of the gene sets associated with IFN-γ response in cells treated with BRAFi + MEKi. NES, normalized enrichment score. FDR: false discovery rate.

(C) Ridgeplot of significantly upregulated Reactome pathways in *ex vivo* isolated cells treated with BRAFi + MEKi compared to control.

(D) Visualization of PD-1 signaling network.

(E) Individual MHC genes were upregulated in murine glioma cells with BRAFi (dabrafenib) + MEKi (trametinib) treatment.

(F) Relative expression of MHC genes in murine BRaf VE Ink -/ - glioma cell line 419 at 48 hrs. treatment with vehicle control (DMSO) and BRAFi dabrafenib and MEKi trametinib

(D+T) assessed by qRT-PCR. Data shown as mean ± SEM of at least 3 independent experiments. *P < 0.05 as determined by unpaired t-test.

Figure 6:

(A) Representative images of immunofluorescence staining for CTLA-4, CD8, and CD4 in syngeneic orthotopic murine BRaf V600E mutated CDKN2A deleted orthotopic gliomas. DAPI stains DNA in blue. Scale bar, 5 μM.

(B) Quantification of cell populations in (A).

Representative images of immunofluorescence staining for CD8, CD4, and Foxp3 in syngeneic orthotopic murine BRaf V600E mutated CDKN2A deleted orthotopic gliomas. DAPI stains DNA in blue. Scale bar, 20 mM.

(D) Quantification of cell populations in (C).

(E) Representative images of immunofluorescence staining for PDL1 and Nestin in syngeneic orthotopic murine BRaf V600E mutated CDKN2A deleted orthotopic gliomas. DAPI stains DNA in blue. Scale bar, 2 μM.

(F) Quantification of cell populations in (E).

(G) Representative staining of BRAF V600E-mutated CDKN2A deleted high-grade astrocytoma with H&E, and antibodies against BRAF V600E and PD-L1.

Figure 7

(A) Schematic of treatment regimen of syngeneic mice carrying orthotopic BRAF V600E mutated CDKN2A deleted gliomas with dabrafenib (BRAFi/D; 2.5 mg/kg i.p. daily), and trametinib (MEKi/T; 1 mg/kg p.o. daily), anti-PD-1 (α-PD-1; 4 mg/kg i.p. every 2 days)

and anti-CTLA4 (α-CTLA-4; 8 mg/kg at day 1; then 2 mg/kg i.p. every 2 days) antibodies (top). Vehicle treatment with DMSO was used as control and treatment lasted 14 days for the first cohort analyzed by mass cytometry, and until endpoint for the second cohort (survival).

(B) Representative t-distributed stochastic neighbor embedding (tSNE) map of cell populations (bottom).

(C) Representative CyTOF viSNE plots depicting the relative expression levels of CD8a, CD4, PD-1 and CTLA-4 of syngeneic, orthotopic BRAF V600E mutated CDKN2A deleted gliomas from the four treatment groups.

(D) Graphs depicting the frequency of PD-1+ CD8+ and PD1+CD4+ (top) or CTLA-4+ CD8+ or CTLA4+CD4+ (bottom) T cells normalized to control/Ctrl. *$P < 0.05$ as assessed by one-way ANOVA with Dunnett's multiple comparisons test. Data representative of two independent experiments.

(E) Kaplan-Meier survival curve of immunocompetent mice with orthotopic BRAF V600E mutated CDKN2A deleted gliomas treated as described in (A). The red arrow indicates the treatment initiation at day 30.

(F) Kaplan-Meier survival curve in immunocompromised (athymic) mice with orthotopic BRaf VE Ink-/- gliomas treated with dabrafenib (2.5 mg/kg i.p. daily), trametinib (0.3 mg/kg p.o. daily), α-PD-L1 (20 mg/kg at day 1; then 8 mg/kg i.p. every 3 days), α-CTLA-4 (8 mg/kg at day 1; then 2 mg/kg i.p. every 3 days) or a combination until animal subjects succumbed to the tumor. The black arrow indicates the treatment initiation at day 14.

Tables

Table 1. List of tumor subclasses, major genetic events, and number of tumors analyzed for each subclass (n) in **Fig. 6E.**

Table 2: Number of mice, median survival, and statistical analyses by the log-rank test in Figs. 7E and 7F.

References and Notes

1. Ostrom, Q.T., et al., *CBTRUS Statistical Report: Primary Brain and Other Central Nervous System Tumors Diagnosed in the United States in 2011-2015.* Neuro Oncol, 2018. **20**(suppl_4): p. iv1-iv86.
2. Ostrom, Q.T., et al., *CBTRUS Statistical Report: Primary Brain and Other Central Nervous System Tumors Diagnosed in the United States in 2012-2016.* Neuro Oncol, 2019. **21**(Supplement_5): p. v1-v100.
3. Balss, J., et al., *Analysis of the IDH1 codon 132 mutation in brain tumors.* Acta Neuropathol, 2008. **116**(6): p. 597-602.
4. Parsons, D.W., et al., *An integrated genomic analysis of human glioblastoma multiforme.* Science, 2008. **321**(5897): p. 1807-12.
5. Yan, H., et al., *IDH1 and IDH2 mutations in gliomas.* N Engl J Med, 2009. **360**(8): p. 765-73.
6. Ryall, S., et al., *Integrated Molecular and Clinical Analysis of 1,000 Pediatric Low-Grade Gliomas.* Cancer Cell, 2020. **37**(4): p. 569-583 e5.
7. Schindler, G., et al., *Analysis of BRAF V600E mutation in 1,320 nervous system tumors reveals high mutation frequencies in pleomorphic xanthoastrocytoma, ganglioglioma and extra-cerebellar pilocytic astrocytoma.* Acta Neuropathol, 2011. **121**(3): p. 397-405.
8. Dahiya, S., et al., *BRAF-V600E mutation in pediatric and adult glioblastoma.* Neuro Oncol, 2014. **16**(2): p. 318-9.
9. Nobre, L., et al., *Outcomes of BRAF V600E Pediatric Gliomas Treated With Targeted BRAF Inhibition.* JCO Precis Oncol, 2020. **4**.
10. Wan, P.T., et al., *Mechanism of activation of the RAF-ERK signaling pathway by oncogenic mutations of B-RAF.* Cell, 2004. **116**(6): p. 855-67.
11. Davies, H., et al., *Mutations of the BRAF gene in human cancer.* Nature, 2002. **417**(6892): p. 949-54.

12. Raabe, E.H., et al., *BRAF activation induces transformation and then senescence in human neural stem cells: a pilocytic astrocytoma model.* Clin Cancer Res, 2011. **17**(11): p. 3590-9.
13. Jacob, K., et al., *Genetic aberrations leading to MAPK pathway activation mediate oncogene-induced senescence in sporadic pilocytic astrocytomas.* Clin Cancer Res, 2011. **17**(14): p. 4650-60.
14. Kleinschmidt-DeMasters, B.K., et al., *Epithelioid GBMs show a high percentage of BRAF V600E mutation.* Am J Surg Pathol, 2013. **37**(5): p. 685-98.
15. Jones, D.T.W., et al., *Pediatric low-grade gliomas: next biologically driven steps.* Neuro Oncol, 2018. **20**(2): p. 160-173.
16. Packer, R.J., et al., *Pediatric low-grade gliomas: implications of the biologic era.* Neuro Oncol, 2017. **19**(6): p. 750-761.
17. Stokland, T., et al., *A multivariate analysis of factors determining tumor progression in childhood low-grade glioma: a population-based cohort study (CCLG CNS9702).* Neuro Oncol, 2010. **12**(12): p. 1257-68.
18. Zhang, J., et al., *Whole-genome sequencing identifies genetic alterations in pediatric low-grade gliomas.* Nat Genet, 2013. **45**(6): p. 602-12.
19. Dahiya, S., et al., *BRAF(V600E) mutation is a negative prognosticator in pediatric ganglioglioma.* Acta Neuropathol, 2013. **125**(6): p. 901-10.
20. Lassaletta, A., et al., *Therapeutic and Prognostic Implications of BRAF V600E in Pediatric Low-Grade Gliomas.* J Clin Oncol, 2017. **35**(25): p. 2934-2941.
21. Mistry, M., et al., *BRAF mutation and CDKN2A deletion define a clinically distinct subgroup of childhood secondary high-grade glioma.* J Clin Oncol, 2015. **33**(9): p. 1015-22.
22. Stupp, R., et al., *Effects of radiotherapy with concomitant and adjuvant temozolomide versus radiotherapy alone on survival in glioblastoma in a randomised phase III study: 5-year analysis of the EORTC-NCIC trial.* Lancet Oncol, 2009. **10**(5): p. 459-66.
23. Jones, C., et al., *Pediatric high-grade glioma: biologically and clinically in need of new thinking.* Neuro Oncol, 2017. **19**(2): p. 153-161.
24. de Blank, P., et al., *Management of pediatric low-grade glioma.* Curr Opin Pediatr, 2019. **31**(1): p. 21-27.
25. Schreck, K.C., S.A. Grossman, and C.A. Pratilas, *BRAF Mutations and the Utility of RAF and MEK Inhibitors in Primary Brain Tumors.* Cancers (Basel), 2019. **11**(9).
26. Cohen, Y., et al., *BRAF mutation in papillary thyroid carcinoma.* J Natl Cancer Inst, 2003. **95**(8): p. 625-7.
27. Bollag, G., et al., *Clinical efficacy of a RAF inhibitor needs broad target blockade in BRAF-mutant melanoma.* Nature, 2010. **467**(7315): p. 596-9.
28. Chapman, P.B., et al., *Improved survival with vemurafenib in melanoma with BRAF V600E mutation.* N Engl J Med, 2011. **364**(26): p. 2507-16.
29. Yang, H., et al., *Antitumor activity of BRAF inhibitor vemurafenib in preclinical models of BRAF-mutant colorectal cancer.* Cancer Res, 2012. **72**(3): p. 779-89.
30. Sullivan, R., et al., *Achievements and challenges of molecular targeted therapy in melanoma.* Am Soc Clin Oncol Educ Book, 2015: p. 177-86.
31. Bai, X. and K.T. Flaherty, *Targeted and immunotherapies in BRAF mutant melanoma: where we stand and what to expect.* Br J Dermatol, 2021. **185**(2): p. 253-262.

32. Brose, M.S., et al., *Vemurafenib in patients with BRAF(V600E)-positive metastatic or unresectable papillary thyroid cancer refractory to radioactive iodine: a non-randomised, multicentre, open-label, phase 2 trial.* Lancet Oncol, 2016. **17**(9): p. 1272-82.
33. Kopetz, S., et al., *Phase II Pilot Study of Vemurafenib in Patients With Metastatic BRAF-Mutated Colorectal Cancer.* J Clin Oncol, 2015. **33**(34): p. 4032-8.
34. Tiacci, E., et al., *Targeting Mutant BRAF in Relapsed or Refractory Hairy-Cell Leukemia.* N Engl J Med, 2015. **373**(18): p. 1733-47.
35. Subbiah, V., et al., *Pan-Cancer Efficacy of Vemurafenib in BRAF (V600)-Mutant Non-Melanoma Cancers.* Cancer Discov, 2020. **10**(5): p. 657-663.
36. Hargrave, D.R., et al., *Efficacy and Safety of Dabrafenib in Pediatric Patients with BRAF V600 Mutation-Positive Relapsed or Refractory Low-Grade Glioma: Results from a Phase I/IIa Study.* Clin Cancer Res, 2019. **25**(24): p. 7303-7311.
37. Kieran, M.W., et al., *A Phase I and Pharmacokinetic Study of Oral Dabrafenib in Children and Adolescent Patients with Recurrent or Refractory BRAF V600 Mutation-Positive Solid Tumors.* Clin Cancer Res, 2019. **25**(24): p. 7294-7302.
38. Nicolaides, T., et al., *Phase I study of vemurafenib in children with recurrent or progressive BRAF(V600E) mutant brain tumors: Pacific Pediatric Neuro-Oncology Consortium study (PNOC-002).* Oncotarget, 2020. **11**(21): p. 1942-1952.
39. Wang, H., et al., *Population Pharmacokinetics of Vemurafenib in Children With Recurrent/Refractory BRAF Gene V600E-Mutant Astrocytomas.* J Clin Pharmacol, 2020. **60**(9): p. 1209-1219.
40. Lerner, R.G., et al., *Targeting a Plk1-Controlled Polarity Checkpoint in Therapy-Resistant Glioblastoma-Propagating Cells.* Cancer Res, 2015. **75**(24): p. 5355-66.
41. Huillard, E., et al., *Cooperative interactions of BRAFV600E kinase and CDKN2A locus deficiency in pediatric malignant astrocytoma as a basis for rational therapy.* Proc Natl Acad Sci U S A, 2012. **109**(22): p. 8710-5.
42. Grossauer, S., et al., *Concurrent MEK targeted therapy prevents MAPK pathway reactivation during BRAFV600E targeted inhibition in a novel syngeneic murine glioma model.* Oncotarget, 2016. **7**(46): p. 75839-75853.
43. Subbiah, V., Stein, A., van den Bent, M., Wick, A., de Vos, F. Y., von Bubnoff, N., van Linde, M.E., Lai, A., Prager, G. W., Campone, M., Fasolo, A., Lopez-Martin, J. A., Kim, T. M., Hofheinz, R.D., Blay, J.Y., Cho, D.C., Gazzah, A., Pouessel, D., Yachnin, J., Boran, A., Burgess, P., Ilankumaran, P., Gasal., D., and Wen, P.Y,, *Dabrafenib plus trametinib in BRAF V600E-mutant high-grade (HGG) and low-grade glima (LGG). .* Cancer Research, 2021. **81**(13).
44. Nicolaides, T.P., et al., *Targeted therapy for BRAFV600E malignant astrocytoma.* Clin Cancer Res, 2011. **17**(24): p. 7595-604.
45. Yao, T.W., et al., *Acquired resistance to BRAF inhibition in BRAFV600E mutant gliomas.* Oncotarget, 2017. **8**(1): p. 583-595.
46. Ascierto, P.A., et al., *Cobimetinib combined with vemurafenib in advanced BRAF(V600)-mutant melanoma (coBRIM): updated efficacy results from a randomised, double-blind, phase 3 trial.* Lancet Oncol, 2016. **17**(9): p. 1248-60.
47. Flaherty, K.T., et al., *Combined BRAF and MEK inhibition in melanoma with BRAF V600 mutations.* N Engl J Med, 2012. **367**(18): p. 1694-703.

48. Johanns, T.M., et al., *Rapid Clinical and Radiographic Response With Combined Dabrafenib and Trametinib in Adults With BRAF-Mutated High-Grade Glioma.* J Natl Compr Canc Netw, 2018. **16**(1): p. 4-10.
49. Odogwu, L., et al., *FDA Approval Summary: Dabrafenib and Trametinib for the Treatment of Metastatic Non-Small Cell Lung Cancers Harboring BRAF V600E Mutations.* Oncologist, 2018. **23**(6): p. 740-745.
50. Toll, S.A., et al., *Sustained response of three pediatric BRAF(V600E) mutated high-grade gliomas to combined BRAF and MEK inhibitor therapy.* Oncotarget, 2019. **10**(4): p. 551-557.
51. Chen, G., et al., *Clinical, Molecular, and Immune Analysis of Dabrafenib-Trametinib Combination Treatment for BRAF Inhibitor-Refractory Metastatic Melanoma: A Phase 2 Clinical Trial.* JAMA Oncol, 2016. **2**(8): p. 1056-64.
52. Brown, N.F., et al., *Dabrafenib and trametinib in BRAFV600E mutated glioma.* CNS Oncol, 2017. **6**(4): p. 291-296.
53. Marks, A.M., et al., *Response to the BRAF/MEK inhibitors dabrafenib/trametinib in an adolescent with a BRAF V600E mutated anaplastic ganglioglioma intolerant to vemurafenib.* Pediatr Blood Cancer, 2018. **65**(5): p. e26969.
54. Rayi, A., et al., *Targeted Therapy for BRAF Mutant Brain Tumors.* Curr Treat Options Oncol, 2021. **22**(11): p. 105.
55. Mackay, A., et al., *Molecular, Pathological, Radiological, and Immune Profiling of Non-brainstem Pediatric High-Grade Glioma from the HERBY Phase II Randomized Trial.* Cancer Cell, 2018. **33**(5): p. 829-842 e5.
56. Mackay, A., et al., *Integrated Molecular Meta-Analysis of 1,000 Pediatric High-Grade and Diffuse Intrinsic Pontine Glioma.* Cancer Cell, 2017. **32**(4): p. 520-537 e5.
57. Wen, P.Y., et al., *Dabrafenib plus trametinib in patients with BRAF(V600E)-mutant low-grade and high-grade glioma (ROAR): a multicentre, open-label, single-arm, phase 2, basket trial.* Lancet Oncol, 2022. **23**(1): p. 53-64.
58. Leslie, C., et al., *FOXP3+ T regulatory lymphocytes in primary melanoma are associated with BRAF mutation but not with response to BRAF inhibitor.* Pathology, 2015. **47**(6): p. 557-63.
59. Shabaneh, T.B., et al., *Oncogenic BRAF(V600E) Governs Regulatory T-cell Recruitment during Melanoma Tumorigenesis.* Cancer Res, 2018. **78**(17): p. 5038-5049.
60. Sumimoto, H., et al., *The BRAF-MAPK signaling pathway is essential for cancer-immune evasion in human melanoma cells.* J Exp Med, 2006. **203**(7): p. 1651-6.
61. Wilmott, J.S., et al., *Selective BRAF inhibitors induce marked T-cell infiltration into human metastatic melanoma.* Clin Cancer Res, 2012. **18**(5): p. 1386-94.
62. Hu-Lieskovan, S., et al., *Improved antitumor activity of immunotherapy with BRAF and MEK inhibitors in BRAF(V600E) melanoma.* Sci Transl Med, 2015. **7**(279): p. 279ra41.
63. Boni, A., et al., *Selective BRAFV600E inhibition enhances T-cell recognition of melanoma without affecting lymphocyte function.* Cancer Res, 2010. **70**(13): p. 5213-9.
64. Ho, P.C. and S.M. Kaech, *BRAF-targeted therapy alters the functions of intratumoral CD4(+) T cells to inhibit melanoma progression.* Oncoimmunology, 2014. **3**: p. e29126.
65. Ho, P.C., et al., *Immune-based antitumor effects of BRAF inhibitors rely on signaling by CD40L and IFNgamma.* Cancer Res, 2014. **74**(12): p. 3205-17.
66. Sapkota, B., C.E. Hill, and B.P. Pollack, *Vemurafenib enhances MHC induction in BRAF(V600E) homozygous melanoma cells.* Oncoimmunology, 2013. **2**(1): p. e22890.

67. Wei, S.C., C.R. Duffy, and J.P. Allison, *Fundamental Mechanisms of Immune Checkpoint Blockade Therapy.* Cancer Discov, 2018. **8**(9): p. 1069-1086.
68. Robinson, J.P., et al., *Activated BRAF induces gliomas in mice when combined with Ink4a/Arf loss or Akt activation.* Oncogene, 2010. **29**(3): p. 335-44.
69. Fukuoka, K., et al., *Clinical impact of combined epigenetic and molecular analysis of pediatric low-grade gliomas.* Neuro Oncol, 2020. **22**(10): p. 1474-1483.
70. Korshunov, A., et al., *Integrated analysis of pediatric glioblastoma reveals a subset of biologically favorable tumors with associated molecular prognostic markers.* Acta Neuropathol, 2015. **129**(5): p. 669-78.
71. Dankort, D., et al., *A new mouse model to explore the initiation, progression, and therapy of BRAFV600E-induced lung tumors.* Genes Dev, 2007. **21**(4): p. 379-84.
72. Aguirre, A.J., et al., *Activated Kras and Ink4a/Arf deficiency cooperate to produce metastatic pancreatic ductal adenocarcinoma.* Genes Dev, 2003. **17**(24): p. 3112-26.
73. Ligon, K.L., et al., *The oligodendroglial lineage marker OLIG2 is universally expressed in diffuse gliomas.* J Neuropathol Exp Neurol, 2004. **63**(5): p. 499-509.
74. Marques, S., et al., *Oligodendrocyte heterogeneity in the mouse juvenile and adult central nervous system.* Science, 2016. **352**(6291): p. 1326-1329.
75. Koh, H.Y., et al., *BRAF somatic mutation contributes to intrinsic epileptogenicity in pediatric brain tumors.* Nat Med, 2018. **24**(11): p. 1662-1668.
76. Ludwig, K. and H.I. Kornblum, *Molecular markers in glioma.* J Neurooncol, 2017. **134**(3): p. 505-512.
77. Setoguchi, T. and T. Kondo, *Nuclear export of OLIG2 in neural stem cells is essential for ciliary neurotrophic factor-induced astrocyte differentiation.* J Cell Biol, 2004. **166**(7): p. 963-8.
78. Reitman, Z.J., et al., *Mitogenic and progenitor gene programmes in single pilocytic astrocytoma cells.* Nat Commun, 2019. **10**(1): p. 3731.
79. Sugiarto, S., et al., *Asymmetry-defective oligodendrocyte progenitors are glioma precursors.* Cancer Cell, 2011. **20**(3): p. 328-40.
80. Ben-Porath, I., et al., *An embryonic stem cell-like gene expression signature in poorly differentiated aggressive human tumors.* Nat Genet, 2008. **40**(5): p. 499-507.
81. Bao, S., et al., *Glioma stem cells promote radioresistance by preferential activation of the DNA damage response.* Nature, 2006. **444**(7120): p. 756-60.
82. Rich, J.N. and S. Bao, *Chemotherapy and cancer stem cells.* Cell Stem Cell, 2007. **1**(4): p. 353-5.
83. Hemmati, H.D., et al., *Cancerous stem cells can arise from pediatric brain tumors.* Proc Natl Acad Sci U S A, 2003. **100**(25): p. 15178-83.
84. Vella, L.J., et al., *MEK inhibition, alone or in combination with BRAF inhibition, affects multiple functions of isolated normal human lymphocytes and dendritic cells.* Cancer Immunol Res, 2014. **2**(4): p. 351-60.
85. Vella, L.J., et al., *The kinase inhibitors dabrafenib and trametinib affect isolated immune cell populations.* Oncoimmunology, 2014. **3**(7): p. e946367.
86. Kono, M., et al., *Role of the mitogen-activated protein kinase signaling pathway in the regulation of human melanocytic antigen expression.* Mol Cancer Res, 2006. **4**(10): p. 779-92.
87. Quail, D.F. and J.A. Joyce, *The Microenvironmental Landscape of Brain Tumors.* Cancer Cell, 2017. **31**(3): p. 326-341.

88. Castro, F., et al., *Interferon-Gamma at the Crossroads of Tumor Immune Surveillance or Evasion.* Front Immunol, 2018. **9**: p. 847.
89. Kumar, A., et al., *CXCL14 Promotes a Robust Brain Tumor-Associated Immune Response in Glioma.* Clin Cancer Res, 2022. **28**(13): p. 2898-2910.
90. Krishnatry, R., et al., *Clinical and treatment factors determining long-term outcomes for adult survivors of childhood low-grade glioma: A population-based study.* Cancer, 2016. **122**(8): p. 1261-9.
91. Nageswara Rao, A.A. and R.J. Packer, *Advances in the management of low-grade gliomas.* Curr Oncol Rep, 2014. **16**(8): p. 398.
92. Wisoff, J.H., et al., *Primary neurosurgery for pediatric low-grade gliomas: a prospective multi-institutional study from the Children's Oncology Group.* Neurosurgery, 2011. **68**(6): p. 1548-54; discussion 1554-5.
93. Cases-Cunillera, S., et al., *Heterogeneity and excitability of BRAFV600E-induced tumors is determined by Akt/mTOR-signaling state and Trp53-loss.* Neuro Oncol, 2022. **24**(5): p. 741-754.
94. Lyustikman, Y., et al., *Constitutive activation of Raf-1 induces glioma formation in mice.* Neoplasia, 2008. **10**(5): p. 501-10.
95. Shin, C.H., et al., *The BRAF kinase domain promotes the development of gliomas in vivo.* Genes Cancer, 2015. **6**(1-2): p. 9-18.
96. Galabova-Kovacs, G., et al., *Essential role of B-Raf in oligodendrocyte maturation and myelination during postnatal central nervous system development.* J Cell Biol, 2008. **180**(5): p. 947-55.
97. Li, S., et al., *RAS/ERK signaling controls proneural genetic programs in cortical development and gliomagenesis.* J Neurosci, 2014. **34**(6): p. 2169-90.
98. Hawkins, C.E., U. Bartels, and E. Bouffet, *Molecular genetic approaches and potential new therapeutic strategies for pediatric diffuse intrinsic pontine glioma.* J Clin Oncol, 2011. **29**(30): p. 3956-7.
99. Bouffet, E., et al., *Phase II study of weekly vinblastine in recurrent or refractory pediatric low-grade glioma.* J Clin Oncol, 2012. **30**(12): p. 1358-63.
100. Lassaletta, A., et al., *Phase II Weekly Vinblastine for Chemotherapy-Naive Children With Progressive Low-Grade Glioma: A Canadian Pediatric Brain Tumor Consortium Study.* J Clin Oncol, 2016. **34**(29): p. 3537-3543.
101. Andor, N., et al., *Pan-cancer analysis of the extent and consequences of intratumor heterogeneity.* Nat Med, 2016. **22**(1): p. 105-13.
102. Andor, N., et al., *EXPANDS: expanding ploidy and allele frequency on nested subpopulations.* Bioinformatics, 2014. **30**(1): p. 50-60.
103. Tirosh, I., et al., *Single-cell RNA-seq supports a developmental hierarchy in human oligodendroglioma.* Nature, 2016. **539**(7628): p. 309-313.
104. Gojo, J., et al., *Single-Cell RNA-Seq Reveals Cellular Hierarchies and Impaired Developmental Trajectories in Pediatric Ependymoma.* Cancer Cell, 2020. **38**(1): p. 44-59 e9.
105. Neftel, C., et al., *An Integrative Model of Cellular States, Plasticity, and Genetics for Glioblastoma.* Cell, 2019. **178**(4): p. 835-849 e21.
106. Chen, R., et al., *KIAA1549-BRAF Expression Establishes a Permissive Tumor Microenvironment Through NFkappaB-Mediated CCL2 Production.* Neoplasia, 2019. **21**(1): p. 52-60.

107. Kaul, A., et al., *Conditional KIAA1549:BRAF mice reveal brain region- and cell type-specific effects.* Genesis, 2013. **51**(10): p. 708-16.
108. Liu, G., et al., *Analysis of gene expression and chemoresistance of CD133+ cancer stem cells in glioblastoma.* Mol Cancer, 2006. **5**: p. 67.
109. Miraglia, S., et al., *A novel five-transmembrane hematopoietic stem cell antigen: isolation, characterization, and molecular cloning.* Blood, 1997. **90**(12): p. 5013-21.
110. Yin, A.H., et al., *AC133, a novel marker for human hematopoietic stem and progenitor cells.* Blood, 1997. **90**(12): p. 5002-12.
111. Uchida, N., et al., *Direct isolation of human central nervous system stem cells.* Proc Natl Acad Sci U S A, 2000. **97**(26): p. 14720-5.
112. Bhat, K.P.L., et al., *Mesenchymal differentiation mediated by NF-kappaB promotes radiation resistance in glioblastoma.* Cancer Cell, 2013. **24**(3): p. 331-46.
113. Flavahan, W.A., et al., *Brain tumor initiating cells adapt to restricted nutrition through preferential glucose uptake.* Nat Neurosci, 2013. **16**(10): p. 1373-82.
114. Hoang-Minh, L.B., et al., *Infiltrative and drug-resistant slow-cycling cells support metabolic heterogeneity in glioblastoma.* EMBO J, 2018. **37**(23).
115. Deleyrolle, L.P., et al., *Identification and isolation of slow-dividing cells in human glioblastoma using carboxy fluorescein succinimidyl ester (CFSE).* J Vis Exp, 2012(62).
116. Lathia, J.D., et al., *Distribution of CD133 reveals glioma stem cells self-renew through symmetric and asymmetric cell divisions.* Cell Death Dis, 2011. **2**: p. e200.
117. Cheng, L., et al., *Glioblastoma stem cells generate vascular pericytes to support vessel function and tumor growth.* Cell, 2013. **153**(1): p. 139-52.
118. Hu, B., et al., *Epigenetic Activation of WNT5A Drives Glioblastoma Stem Cell Differentiation and Invasive Growth.* Cell, 2016. **167**(5): p. 1281-1295 e18.
119. Nair, N., et al., *A cancer stem cell model as the point of origin of cancer-associated fibroblasts in tumor microenvironment.* Sci Rep, 2017. **7**(1): p. 6838.
120. Cox, C.V., et al., *Expression of CD133 on leukemia-initiating cells in childhood ALL.* Blood, 2009. **113**(14): p. 3287-96.
121. Hermann, P.C., et al., *Distinct populations of cancer stem cells determine tumor growth and metastatic activity in human pancreatic cancer.* Cell Stem Cell, 2007. **1**(3): p. 313-23.
122. O'Brien, C.A., et al., *A human colon cancer cell capable of initiating tumour growth in immunodeficient mice.* Nature, 2007. **445**(7123): p. 106-10.
123. Singh, S.K., et al., *Identification of human brain tumour initiating cells.* Nature, 2004. **432**(7015): p. 396-401.
124. Shibahara, I., et al., *The expression status of CD133 is associated with the pattern and timing of primary glioblastoma recurrence.* Neuro Oncol, 2013. **15**(9): p. 1151-9.
125. Inoue, T., et al., *Expression of CD133 as a Putative Prognostic Biomarker to Predict Intracranial Dissemination of Primary Spinal Cord Astrocytoma.* World Neurosurg, 2018. **110**: p. e715-e726.
126. Zeppernick, F., et al., *Stem cell marker CD133 affects clinical outcome in glioma patients.* Clin Cancer Res, 2008. **14**(1): p. 123-9.
127. Vora, P., et al., *The Rational Development of CD133-Targeting Immunotherapies for Glioblastoma.* Cell Stem Cell, 2020. **26**(6): p. 832-844 e6.
128. Poulikakos, P.I., et al., *RAF inhibitor resistance is mediated by dimerization of aberrantly spliced BRAF(V600E).* Nature, 2011. **480**(7377): p. 387-90.

129. Rizos, H., et al., *BRAF inhibitor resistance mechanisms in metastatic melanoma: spectrum and clinical impact.* Clin Cancer Res, 2014. **20**(7): p. 1965-77.
130. Sievert, A.J., et al., *Paradoxical activation and RAF inhibitor resistance of BRAF protein kinase fusions characterizing pediatric astrocytomas.* Proc Natl Acad Sci U S A, 2013. **110**(15): p. 5957-62.
131. Schreck, K.C., et al., *Deconvoluting Mechanisms of Acquired Resistance to RAF Inhibitors in BRAF(V600E)-Mutant Human Glioma.* Clin Cancer Res, 2021. **27**(22): p. 6197-6208.
132. Frederick, D.T., et al., *BRAF inhibition is associated with enhanced melanoma antigen expression and a more favorable tumor microenvironment in patients with metastatic melanoma.* Clin Cancer Res, 2013. **19**(5): p. 1225-31.
133. Hugo, W., et al., *Non-genomic and Immune Evolution of Melanoma Acquiring MAPKi Resistance.* Cell, 2015. **162**(6): p. 1271-85.
134. Buchbinder, E.I. and A. Desai, *CTLA-4 and PD-1 Pathways: Similarities, Differences, and Implications of Their Inhibition.* Am J Clin Oncol, 2016. **39**(1): p. 98-106.
135. Bloch, O., et al., *Gliomas promote immunosuppression through induction of B7-H1 expression in tumor-associated macrophages.* Clin Cancer Res, 2013. **19**(12): p. 3165-75.
136. Wintterle, S., et al., *Expression of the B7-related molecule B7-H1 by glioma cells: a potential mechanism of immune paralysis.* Cancer Res, 2003. **63**(21): p. 7462-7.
137. Choi, J., et al., *Combination checkpoint therapy with anti-PD-1 and anti-BTLA results in a synergistic therapeutic effect against murine glioblastoma.* Oncoimmunology, 2021. **10**(1): p. 1956142.
138. Kim, J.E., et al., *Combination Therapy with Anti-PD-1, Anti-TIM-3, and Focal Radiation Results in Regression of Murine Gliomas.* Clin Cancer Res, 2017. **23**(1): p. 124-136.
139. Mathios, D., et al., *Anti-PD-1 antitumor immunity is enhanced by local and abrogated by systemic chemotherapy in GBM.* Sci Transl Med, 2016. **8**(370): p. 370ra180.
140. Wu, A., et al., *Combination anti-CXCR4 and anti-PD-1 immunotherapy provides survival benefit in glioblastoma through immune cell modulation of tumor microenvironment.* J Neurooncol, 2019. **143**(2): p. 241-249.
141. Zeng, J., et al., *Anti-PD-1 blockade and stereotactic radiation produce long-term survival in mice with intracranial gliomas.* Int J Radiat Oncol Biol Phys, 2013. **86**(2): p. 343-9.
142. Reardon, D.A., et al., *Glioblastoma Eradication Following Immune Checkpoint Blockade in an Orthotopic, Immunocompetent Model.* Cancer Immunol Res, 2016. **4**(2): p. 124-35.
143. Wainwright, D.A., et al., *Durable therapeutic efficacy utilizing combinatorial blockade against IDO, CTLA-4, and PD-L1 in mice with brain tumors.* Clin Cancer Res, 2014. **20**(20): p. 5290-301.
144. Miranda, A., et al., *Cancer stemness, intratumoral heterogeneity, and immune response across cancers.* Proc Natl Acad Sci U S A, 2019. **116**(18): p. 9020-9029.
145. Yu, M.W. and D.F. Quail, *Immunotherapy for Glioblastoma: Current Progress and Challenge.* Front Immunol, 2021. **12**: p. 676301.
146. Alexandrov, L.B., et al., *Signatures of mutational processes in human cancer.* Nature, 2013. **500**(7463): p. 415-21.
147. Grobner, S.N., et al., *The landscape of genomic alterations across childhood cancers.* Nature, 2018. **555**(7696): p. 321-327.
148. Gromeier, M., et al., *Very low mutation burden is a feature of inflamed recurrent glioblastomas responsive to cancer immunotherapy.* Nat Commun, 2021. **12**(1): p. 352.

149. Kmiecik, J., et al., *Elevated CD3+ and CD8+ tumor-infiltrating immune cells correlate with prolonged survival in glioblastoma patients despite integrated immunosuppressive mechanisms in the tumor microenvironment and at the systemic level.* J Neuroimmunol, 2013. **264**(1-2): p. 71-83.
150. Sonabend, A.M., C.E. Rolle, and M.S. Lesniak, *The role of regulatory T cells in malignant glioma.* Anticancer Res, 2008. **28**(2B): p. 1143-50.
151. Majzner, R.G., S. Heitzeneder, and C.L. Mackall, *Harnessing the Immunotherapy Revolution for the Treatment of Childhood Cancers.* Cancer Cell, 2017. **31**(4): p. 476-485.
152. Zemek, R.M., et al., *Sensitizing the Tumor Microenvironment to Immune Checkpoint Therapy.* Front Immunol, 2020. **11**: p. 223.
153. Simonds, E.F., et al., *Deep immune profiling reveals targetable mechanisms of immune evasion in immune checkpoint inhibitor-refractory glioblastoma.* J Immunother Cancer, 2021. **9**(6).
154. Catakovic, K., et al., *T cell exhaustion: from pathophysiological basics to tumor immunotherapy.* Cell Commun Signal, 2017. **15**(1): p. 1.
155. Reardon, D.A., et al., *Effect of Nivolumab vs Bevacizumab in Patients With Recurrent Glioblastoma: The CheckMate 143 Phase 3 Randomized Clinical Trial.* JAMA Oncol, 2020. **6**(7): p. 1003-1010.
156. Ott, M., et al., *Profiling of patients with glioma reveals the dominant immunosuppressive axis is refractory to immune function restoration.* JCI Insight, 2020. **5**(17).
157. Merchant, M.S., et al., *Phase I Clinical Trial of Ipilimumab in Pediatric Patients with Advanced Solid Tumors.* Clin Cancer Res, 2016. **22**(6): p. 1364-70.
158. Soriano, P., *Generalized lacZ expression with the ROSA26 Cre reporter strain.* Nat Genet, 1999. **21**(1): p. 70-1.
159. Venkatesh, H.S., et al., *Neuronal Activity Promotes Glioma Growth through Neuroligin-3 Secretion.* Cell, 2015. **161**(4): p. 803-16.
160. Daynac, M., et al., *Lgl1 controls NG2 endocytic pathway to regulate oligodendrocyte differentiation and asymmetric cell division and gliomagenesis.* Nat Commun, 2018. **9**(1): p. 2862.

Acknowledgments:

We are deeply thankful to the patients and their families for surgical tissue donations. We acknowledge Sista Sugiarto, Yoko Hirata, Anne Marie Barrette, Brian Reicholf, Robin Lerner, Caitlynn Tran, Pauline Chu, and Gianna Perez for excellent technical assistance and thank Egbert Lu and Erin Simmons and the UCSF Flow Cytometry Core for initial help with mass cytometry and the UCSF Brain Tumor Tissue Core and Stanford Neuroscience Tissue Bank for providing patient samples.

Funding:

NIH/NCI U54 CA261717 (CKP)

Emerson Collective

BRAF Consortium

Weston Haven Fund

Stanford Maternal & Child Health Research Institute

NIH/NINDS R21 NS099836 (CKP)

NIH R01NS080619 (CKP)

NIH R01 CA164746 (CKP)

NIH R01 CA171610

the WHSDM Seed Grant (CKP, SP)

Author contributions:

Conceptualization: SG, CKP, LMP

Methodology: JWP, SG, WW, CKP

Investigation: JWP, SG, KK, WW, LYX, HL, EN, MIBG, CAG, KF, CW, MD, LM,

Visualization: CG, LMP, CKP, KF, PNH, HV,

Funding acquisition: CKP, LMP, GAG, ML

Resources: SP, MM, GAG, LMP, PNH, HV, ML, CKP

Supervision: CKP

Writing – original draft: JWP, SG, CKP

Writing – review & editing: SG, SP, MM, GAG, CKP

Competing interests: Authors declare that they have no competing interests.

Data and materials availability:

All data are available in the main text or the supplementary materials. Further information and request for resources should be directed to and will be fulfilled by the Lead Contact, Claudia Petritsch (cpetri@stanford.edu). All unique/stable reagents, including BRAF V600E mutant murine cells, generated in this study are available from the Lead Contact with a completed Material Transfer Agreement. RNA-seq data for BRAF V600E mutant cell lines with and without MAPK pathway inhibitors treatment will be deposited in the Gene Expression Omnibus (GEO) and accession number GEO will be released prior to publication.

Additional information:

Financial support details

Stefan Grossauer/Katharina Koeck: R01NS080619

Wei Wang: R01NS080619

Jong-Whi Park: Departmental Funds WHSDM Seed Grant Award, (Women's Health & Sex Differences in Medicine, Stanford Prevention Research Center

Mathieu Daynac: R01CA164746, R01NS080619

Lasse Meyer: German Cancer Research Center, Cancer Biology Master Program

Cesar A. Garcia: MedScholars Award, Stanford University School of Medicine

Claudia K. Petritsch: R01CA164746, R01NS080619, R01CA171610, R21NS099836, UCSF Faculty Practice, Stanford Neurosurgery Departmental Funds, WHSDM Seed Grant Award, (Women's Health & Sex Differences in Medicine, Stanford Prevention Research Center, Emerson Collective, Stanford Maternal & Child Health Research Institute,

Fig 1_Park et al

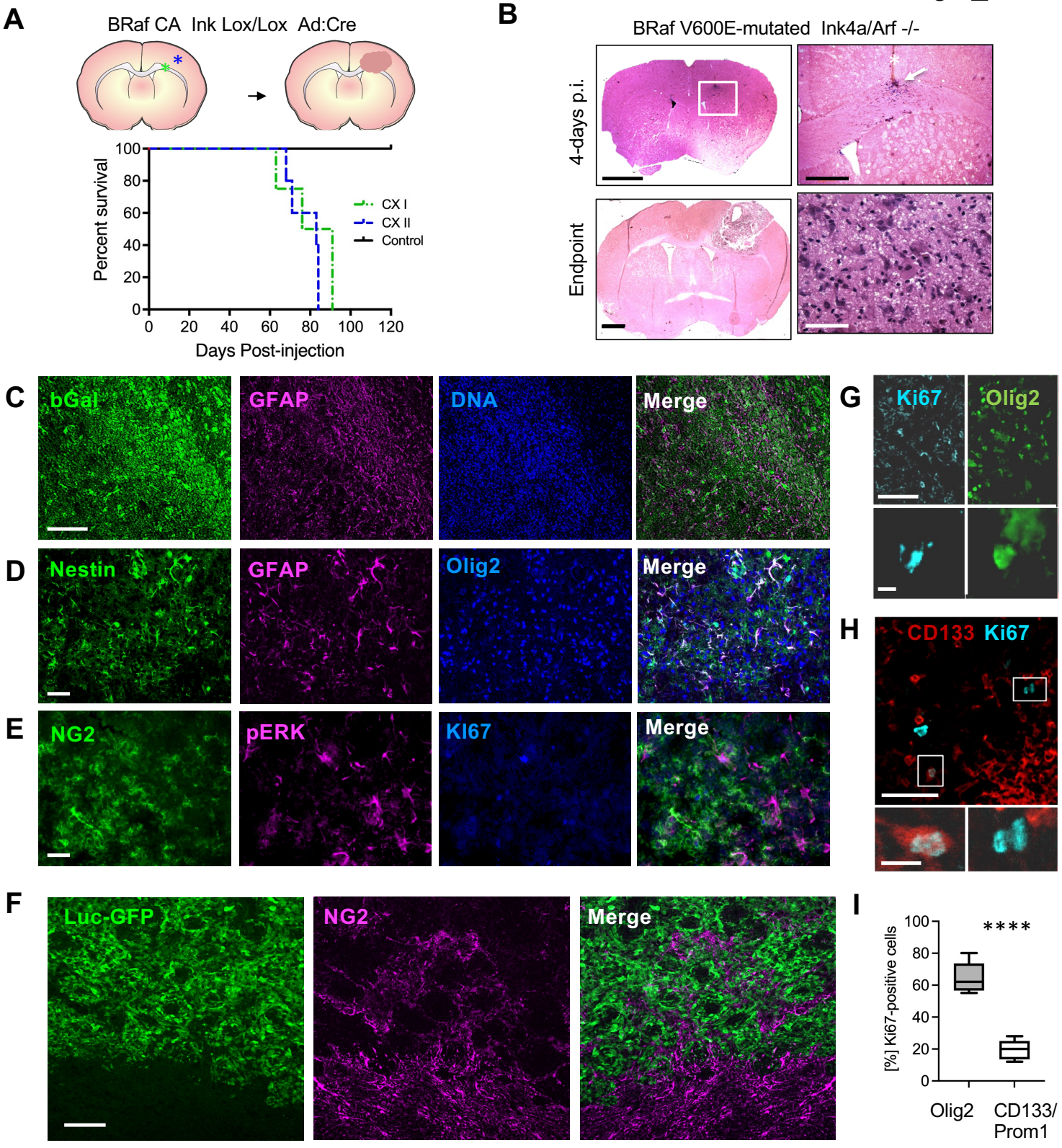

Fig 2_Park et al

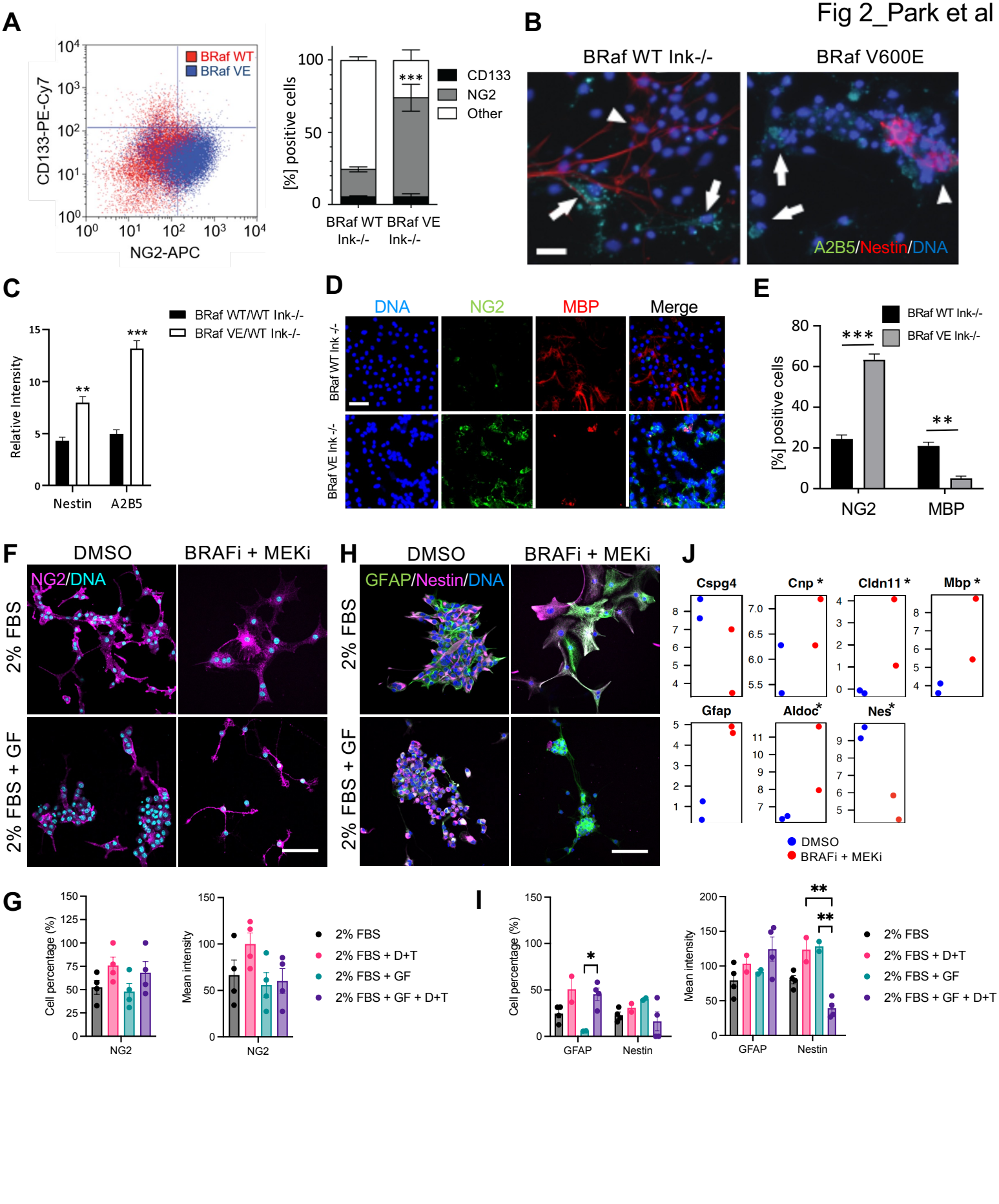

Fig 3_Park et al

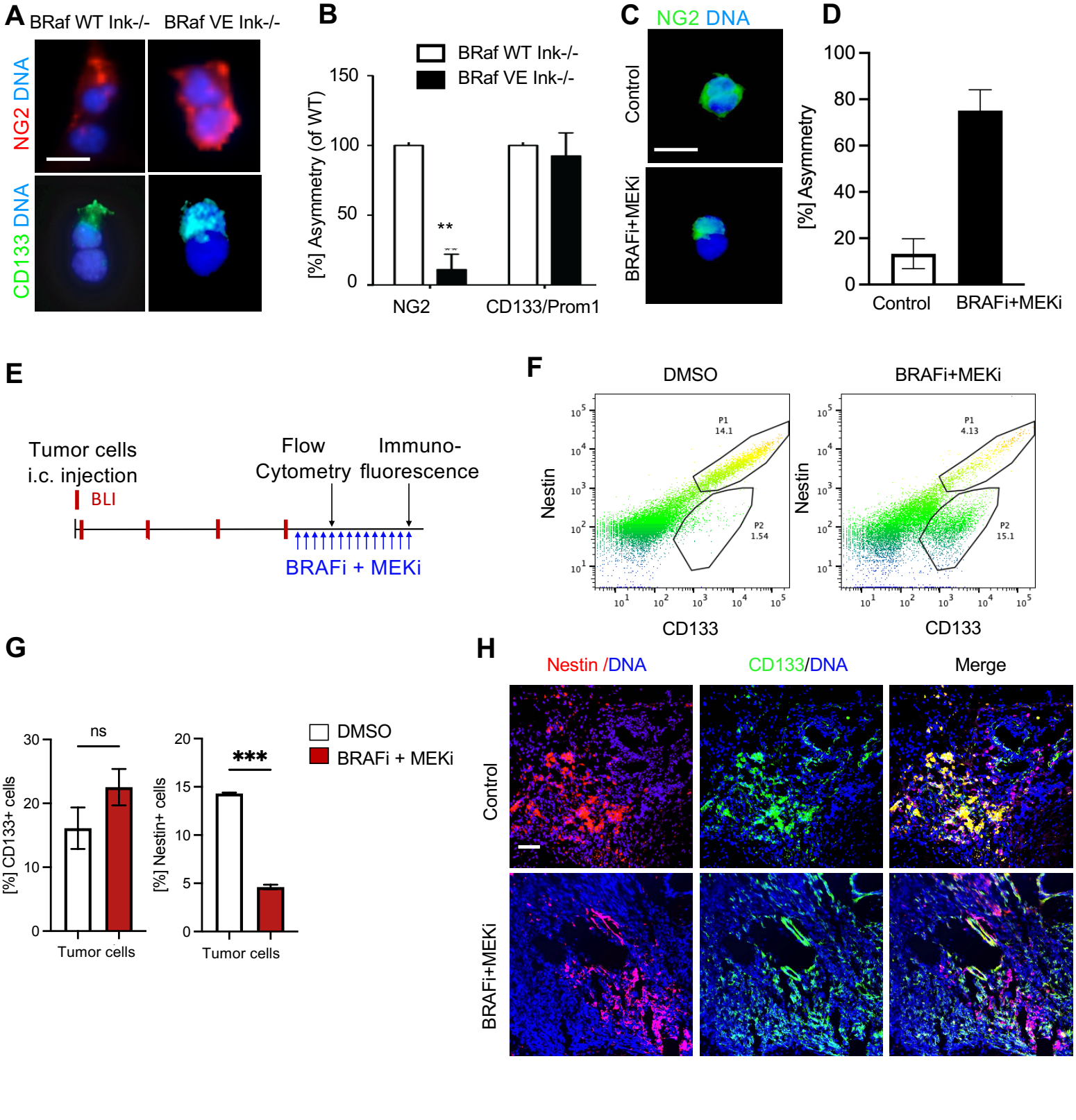

Fig 4_Park et al

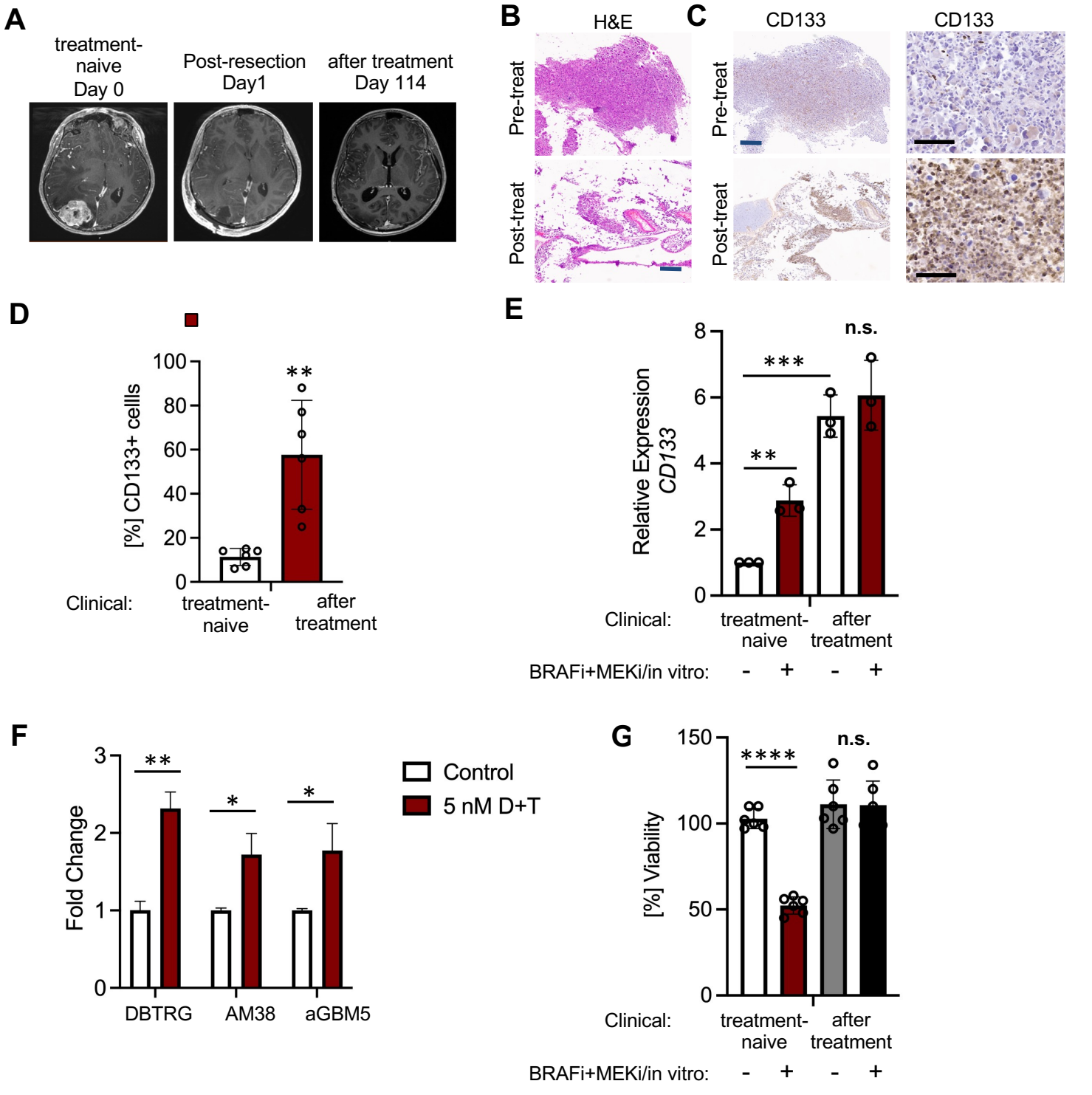

Fig 5_Park et al

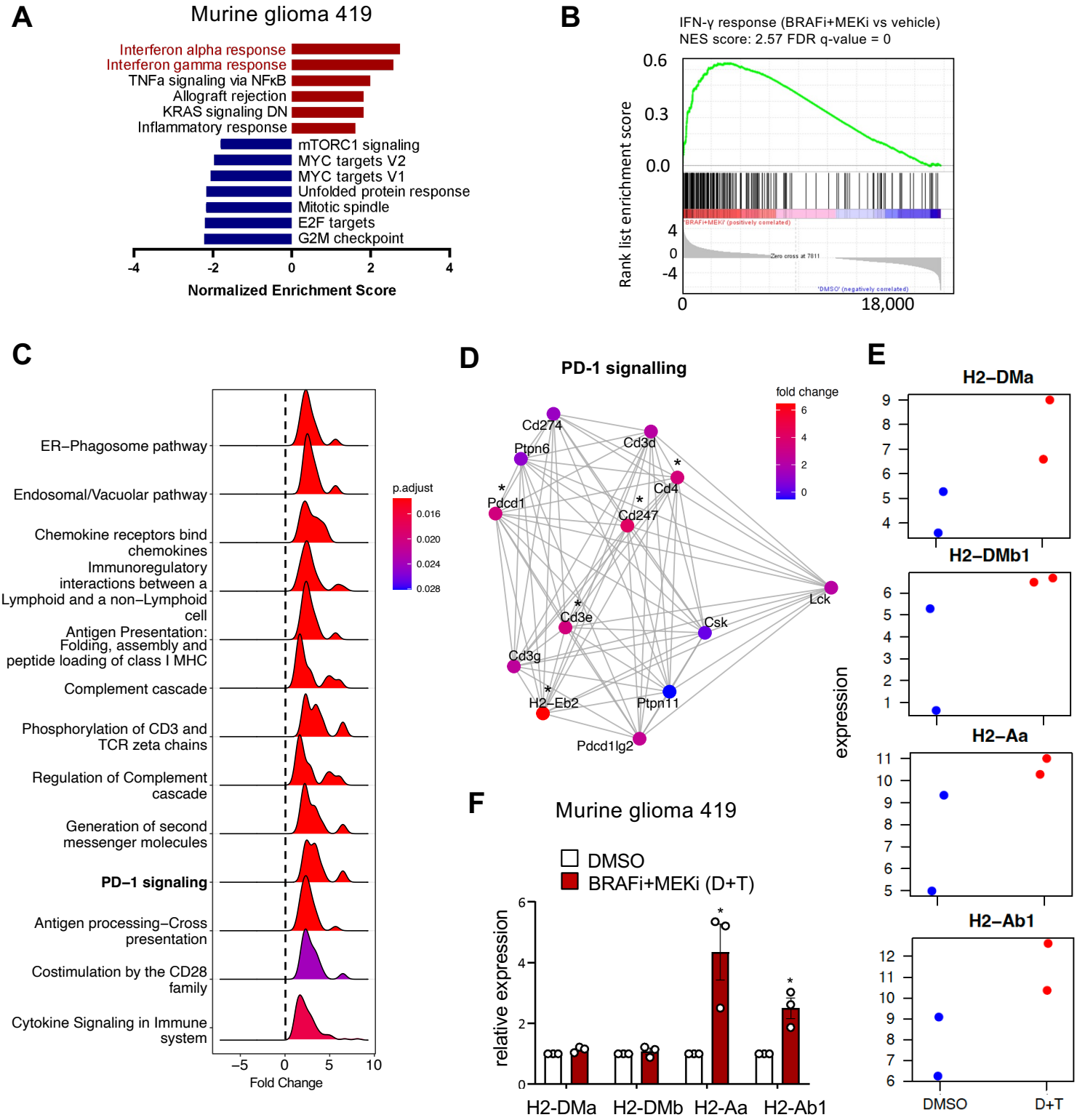

Fig 6_Park et al

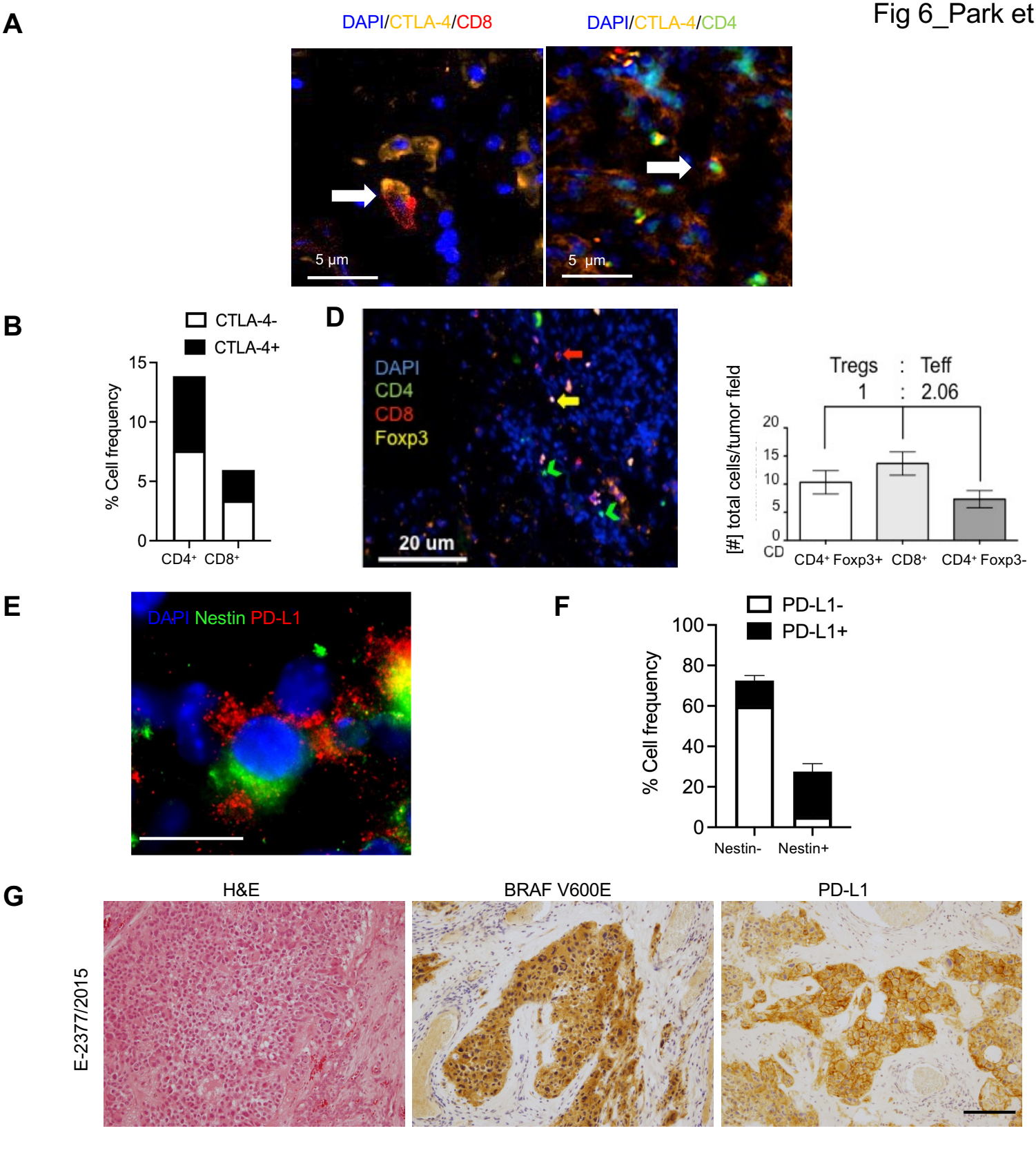

Fig 7_Park et al

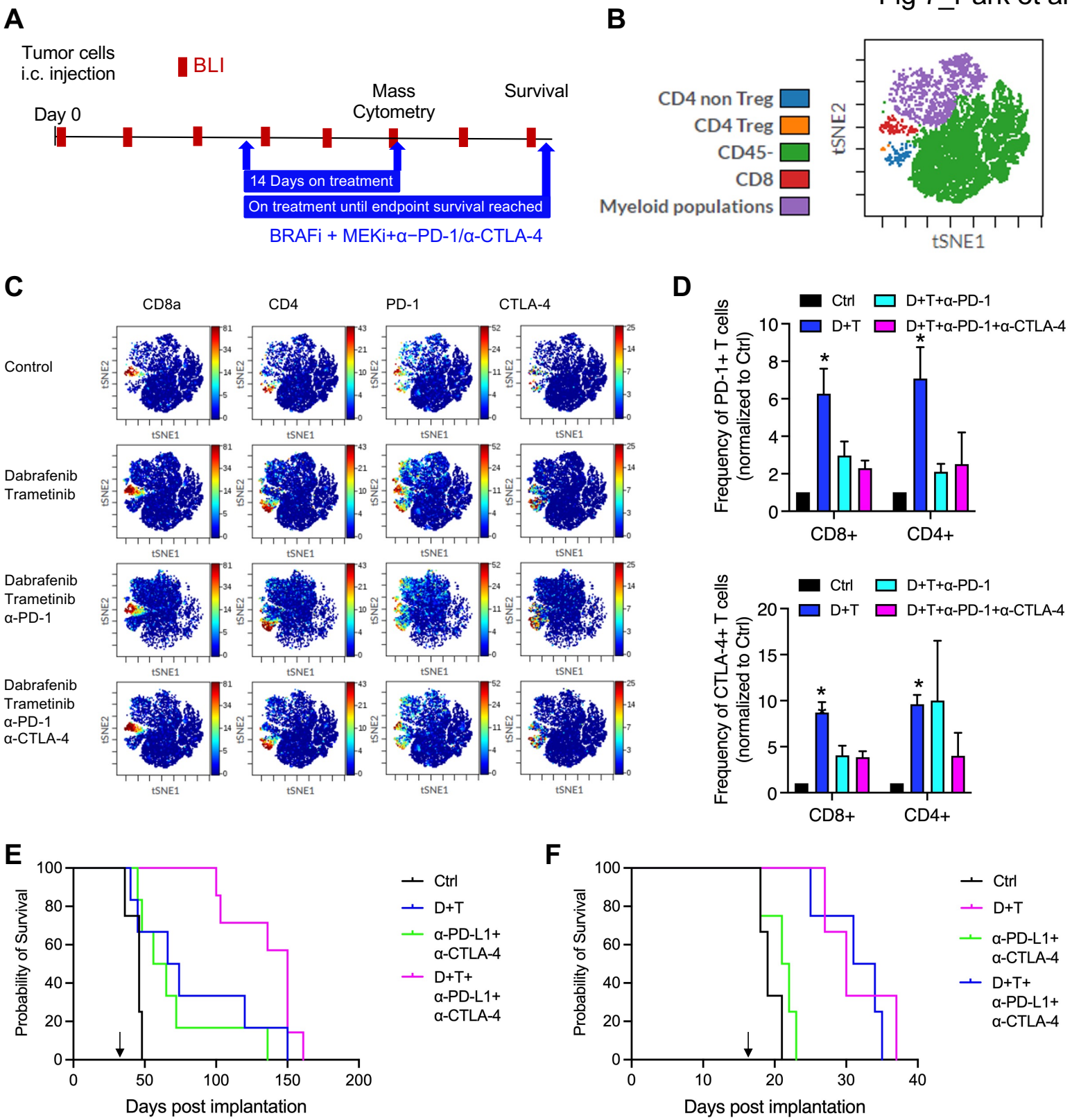

Patient ID	PD-L1 Frequency Score (%)	PD-L1 Intensity Score (%)	PD-L1-Score	Diagnosis
E-338/2017	95	moderate	8	Ganglioglioma
E-1794/2017-2	20	weak	2	Ganglioglioma
E-1869/2014	70	moderate	8	PXA
E-831/2017	90	strong	12	Malignant glioma
E-2377/2015	65	moderate	8	Malignant astrocytoma
E-2012/2014	50	weak	4	PXA

Strain / Group	FVB/N			nu/nu		
	n	**Median survival [d]**	**P value**	**n**	**Median survival [d]**	**P value**
Control	8	46	-	8	19	-
D+T	8	70	*0.049 vs Ctrl	8	30	*0.025 vs Ctrl
α-PD-L1 + α-CTLA-4	8	60.5	*0.036 vs Ctrl 0.489 vs D+T	8	21.5	0.190 vs Ctrl *0.0177 vs D+T
D+T + α-PD-L1 + α-CTLA-4	8	150	***0.0006 vs Ctrl *0.027 vs D+T **0.034 vs α-PD-L1 + α-CTLA-4	8	32.5	*0.010 vs Ctrl 0.727 vs D+T **0.007 vs α-PD-L1 + α-CTLA-4